IEEE Access
Multidisciplinary | Rapid Review | Open Access Journal

Received January 4, 2019, accepted January 17, 2019, date of publication January 25, 2019, date of current version February 14, 2019.

Digital Object Identifier 10.1109/ACCESS.2019.2895210

3D Neuromorphic Wireless Power Transfer and Energy Transmission Based Synaptic Plasticity

BURHAN GULBAHAR[1,2], **(Senior Member, IEEE)**
[1]Department of Electrical and Electronics Engineering, Ozyegin University, 34794 Istanbul, Turkey
[2]Applied Research Center of Technology Products, Ozyegin University, 34794 Istanbul, Turkey

e-mail: burhan.gulbahar@ozyegin.edu.tr

This work was supported by the Vestel Electronics Inc., Manisa, Turkey.

ABSTRACT Energy consumption combined with scalability and 3D architecture is a fundamental constraint for brain-inspired computing. Neuromorphic architectures including memristive, spintronic, and floating gate metal–oxide–semiconductors achieve energy efficiency while having challenges of 3D design and integration, wiring and energy consumption problems for architectures with massive numbers of neurons and synapses. There are bottlenecks due to the integration of communication, memory, and computation tasks while keeping ultra-low energy consumption. In this paper, wireless power transmission (WPT)-based neuromorphic design and theoretical modeling are proposed to solve bottlenecks and challenges. Neuron functionalities with nonlinear activation functions and spiking, synaptic channels, and plasticity rules are designed with magneto-inductive WPT systems. Tasks of communication, computation, memory, and WPT are combined as an all-in-one solution. Numerical analysis is provided for microscale graphene coils in sub-terahertz frequencies with unique neuron design of coils on 2D circular and 3D Goldberg polyhedron substrates as a proof-of-concept satisfying nonlinear activation mechanisms and synaptic weight adaptation. Layered neuromorphic WPT network is utilized to theoretically model and numerically simulate pattern recognition solutions as a simple application of the proposed system design. Finally, open issues and challenges for realizing WPT-based neuromorphic system design are presented including experimental implementations.

INDEX TERMS Neuromorphic, brain-inspired, wireless power transfer, neuron, synaptic channel, magnetic induction, polyhedron, pattern recognition.

I. INTRODUCTION

Energy consumption is one of the fundamental constraints for designing computing platforms mimicking highly energy efficient functioning of the brain with massive number of computation units [1], [2]. Artificial synapses are significantly important to mimic brain and realize nature inspired molecular communications channels [3]. Synaptic plasticity in biological neurons, i.e., adaptation of the synaptic weights in a nervous system in response to surrounding environments [4], is implemented with neuromorphic and analog computing architectures and the adaptation of the synaptic weights based on the relations between pre-synaptic and post-synaptic signals, i.e., plasticity rules, are experimentally realized. They are promising hundreds of femtojoule (fJ) consumption for each spike with implementations of neurons and synapses based on floating gate metal-oxide-semiconductors (MOSs), memristors including resistive random access memory (RRAM) and phase change memory (PCM), and spintronic devices [5]–[8]. However, there are challenges to realize three dimensional (3D) integration of massive amount of neurons and synapses and solving bottlenecks due to integration of wireless communication, memory and computation tasks while keeping energy consumption in ultra-low scales [9], [10]. It is challenging to grasp the fundamental mechanism in brain for reconciling communication and computation [11]. Combining memory and computation tasks is an energy efficient design for next generation architectures such as in-memory computing utilizing resistive switching devices while still utilizing wired architectures including cross-point 3D arrays [12]. Recently, a novel form of energy flow based computing architecture denoted by MIComp is proposed in [13] as a wireless system design combining tasks of wireless magneto-inductive (MI) communication, computation, memory and wireless power transfer (WPT)

2169-3536 © 2019 IEEE. Translations and content mining are permitted for academic research only.
Personal use is also permitted, but republication/redistribution requires IEEE permission.
See http://www.ieee.org/publications_standards/publications/rights/index.html for more information.

with a simple device architecture as all-in-one solution. In this article, the concept of WPT based neuromorphic computation is extended to a unique design and simulation of individual neuron, synaptic channel (SC) and WPT based synaptic plasticity rules with MI channels. Furthermore, the proposed neuromorphic WPT network design is utilized for pattern recognition problems as a practical application where each coil is exploited as a distinct MI neuron modulating the energy flow in the neighborhood.

MI channels with non-radiative magnetic fields have significant advantages for on-chip architectures and multi-node networks [14], [15]. THz frequency resonating oscillations with Faraday's law of induction in multi-layer graphene nanoscale coils are exploited for Tbit/s and ultra-low power wireless communications, and efficient WPT capability [14]. Coupled MI networks are modulated by network topology modulation (NTM) for creating different patterns of energy flow in [16]. These patterns are detected in 3D for computing purposes in [13] by combining single molecule magnets (SMMs) and 2D materials as a promising nanoscale design denoted by MIComp. Each pattern is mapped to a combined operation of communication, computation and memory state allowing 10^{10} to 10^{16} bits in each computation cycle per mm^3 of volume compared with the current transistor counts of on the orders of 10^9 per mm^2 area. Total power dissipation for combined synaptic transmission and neuron processing is targeted to be minimized as an inherent system property for maximizing energy flow and minimization of resistive consumption as the energy flows among neurons. Therefore, decreasing resistive loss in the overall inductive system is promising high performance by utilizing state-of-the-art improvements in material technologies such as intercalated multi-layer graphene coils with higher conductivity and inductance properties [14], [17]. The total power dissipation in a single neuron and SC for a transmission cycle interval is theoretically modeled and numerically simulated for graphene inductor based circuits.

In this article, WPT mechanism defined in MIComp is extended to design building blocks of MI based neuromorphic architecture, i.e., neurons including axon, dendrite, soma and synaptic units, in complete analogy with the biological origin. Furthermore, neuromorphic WPT network design is provided to utilize in solutions of practical pattern recognition problems as a novel application of the unique advantages of WPT. The fundamental requirements for brain analogy are satisfied including scalability, energy efficiency, 3D design, simplicity of building blocks, flexibility in terms of implementation and reorganization, robustness to physical errors while harvesting energy continuously feeding the whole network. In addition, sub-THz speed of operation frequency provides synaptic energy flow with high speed compared with sub-KHz level biological origin. The analogies compared with biological origin are shown in Fig. 1(a) and Table 1 as discussed in detail in Sections II and III. On the other hand, the proposed design has experimental challenges for creating a scalable and energy efficient neuromorphic system as discussed in Section IX. Energy harvesting, switching and alternating voltage source circuits are required to be connected with MI coils as the fundamental unit. The implementation of the building blocks is out of scope of the article while recent technical improvements to utilize in an experimental proof-of-concept neuromorphic WPT system are discussed.

The remainder of the paper is organized as follows. In Section II, contributions and advantages are discussed. In Section III, neuron modeling based on WPT and hardware design are presented. Circuit theoretical modeling is discussed in Section IV. Then, in Sections V and VI, non-linear activation function and energy transmission based synaptic plasticity designs are presented, respectively. In Section VII, neuromorphic WPT system is presented for pattern recognition problems. Then, in Section VIII, numerical analyses for synaptic weight adaptation, activation function implementation and pattern recognition are presented. Finally, in Sections IX and X, open issues and conclusions are given.

II. NEUROMORPHIC WPT ADVANTAGES

Solutions for on-chip computing include promising nanoscale technologies such as combining 3D integration of RRAM and carbon-nanotube field-effect transistors (CNFETs) in [9], neuromorphic architectures including memristor and spintronic designs [6], [8], [10], and various communication oriented bottleneck solutions for the data movement between processing, computation and memory tasks. On-chip wireless communications solutions include radio frequency (RF), optical and MI channel based architectures such as atto-joule opto-electronics in [18], sub-THz MI channel based high performance communications and WPT mechanism with nanoscale inductive coils in [14] and RF based high bandwidth architectures discussed in detail in [14]. MI communication has significant advantages such as combining WPT and communications with ultra-high performances, KHz to sub-THz frequency of resonance capability, high bandwidth, locality without long range interference and support for nanoscale materials with important advantages such as graphene and 2D materials. The contributions, novelties and the advantages of MI neuromorphic computing system compared with the state of the art are summarized as follows:

- *WPT based neuromorphic system:* Implementations of axon, dendrite and soma functions, and synaptic plasticity rules including nonlinearity and activation function are achieved with resonating coil based neuron structures as shown in Fig. 1. MI neuron performs based on WPT as a form of energy flowing model compared with state-of-the-art signaling design. Soma and nucleus functions in terms of generating metabolic energy are implemented with resonating coils generating and relaying energy as shown in Table 1 and Fig. 1(a) [19]. MI WPT is performed between neighbor neurons while ion based signaling is utilized in biological models and signaling based designs are utilized in conventional neuromorphic systems. Activation and triggering with signaling mechanisms in conventional neuromorphic

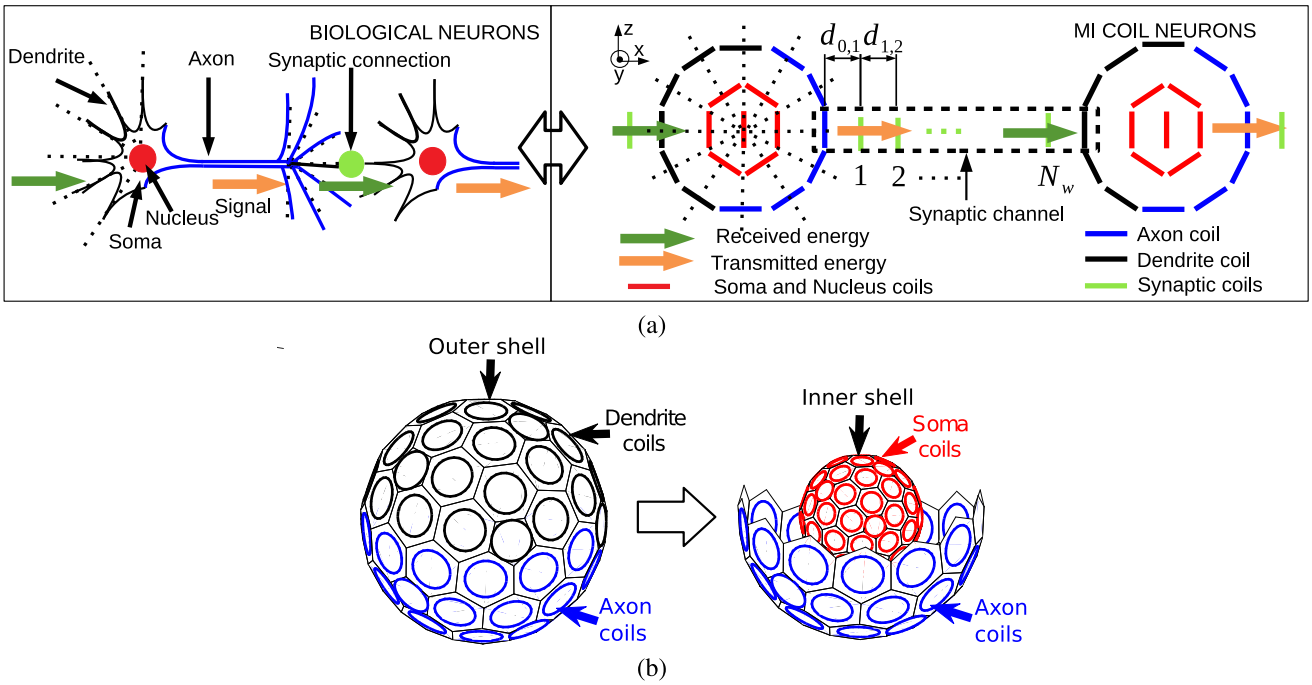

FIGURE 1. (a) Analogy between biological and MI neurons in terms of the functions of the coil groups shown in 2D for simplicity where inter-neuron energy transmission occurs with WPT through a synaptic channel as a MI waveguide. (b) 3D single neuron unit having axon and dendrite coils on the external shell of Goldberg polyhedron with the type $GV(2, 1)$ while soma coils on the inner shell analogical to soma and nucleus cells in biological counterpart.

TABLE 1. Analogy between biological and WPT based magneto-inductive neuromorphic models.

Mechanism	Biological models	Energy transmission based MI Neuromorphic system
Transmission	Signaling	Energy transmission or wireless power transfer (WPT)
Synaptic connections	Scalable	Multiple coils on the neuron shell connecting to multiple neurons with MI WPT
Soma & Nucleus	Energy generation [19]	Adaptive coil topology and/or power levels for energy generation and/or distribution
Simultaneous tasks	All-in-one	Communication, computation, memory, energy transfer and harvesting: all-in-one
Synaptic connections	Adaptive weight	Multi-coil based topology including waveguides (WGs) and adaptive energy transmission
Scalability	Massive	Scalable coil sizes and shell radius allowing massive number of synaptic connections
Geometry	3D, adaptive shaping	3D with arbitrary shaping of synaptic channel, neuron cell and networking
Synaptic speed	Sub-KHz [20]	KHz to sub-THz
Activation function	Nonlinear	Nonlinear, integrate-and-fire for energy transfer, and adaptive with soma topology and energy

architectures do not target energy transfer efficiency while consuming energy in each neuron device without any target to store, to relay the energy or to allow simultaneous wireless information and power transfer (SWIPT). SWIPT is a promising and highly energy efficient wireless system design promising to be utilized in neuromorphic WPT architectures defined in this article [13], [21]. The analogies of all functions are shown in Fig. 1(a) while discussed in detail in Section III.

- *All-in-one system design*: Combination of memory, computation, communication and WPT tasks on the same hardware [13] compared with wired systems combining memory and computation [12] where biological origin achieves all tasks together as shown in Table 1.
- *Intrinsically energy efficient design and harvesting*: WPT based architecture is an intrinsically energy efficient design feeding the network energetically as computation and communication are performed while harvesting saturated energy by utilizing topological MI design as discussed in Section V.
- *Targeting energy transmission efficiency*: The main energy dissipation is in the fixed resistive components of the coils and sources while more complicated loss mechanisms exist in state-of-the-art systems such as memristor based conductance modifications [1]. In the proposed design, resistive components are minimized to reduce consumption on the contrary with memristors including high resistance regime which reduces energy consumption but simultaneously decreasing energy flow [10]. Maximizing energy flow provides a lower bound for consumption as an inherent system design. WPT in a wireless network of neurons allows to utilize network information theoretical optimization tools both temporally and spatially to maximize system energy efficiency [22]. WPT efficiency is high with nanoscale coils and sub-THz WPT [14], compact design and

metamaterials [23]. The power consumption and operation excitation voltage levels are inversely proportional to the efficiency of WPT. It depends on many factors including the material and geometrical properties of the inductive coil, resistive components in the system, noise and the signal-to-noise ratio (SNR) in the receiver coils, mutual inductance between the coils depending on the neuron size and distance, and the consumption in the circuit components for switching, energy storage and voltage generation. The optimization of the power consumption for each synaptic operation is an open issue and future work while the fundamental design principle in the system is to minimize the power dissipating resistive components compared with the traditional architectures.

- *Support for 2D material and single molecule level nanoscale enhancements:* Building blocks of the proposed system include inductors and capacitors which are scalable to nanoscale. 2D materials with significant advantages such as graphene and SMMs are promising to be utilized [14], [24].
- *3D architecture with flexibility:* It allows complex neuromorphic hardware and circuit design routing energy in 3D with arbitrarily oriented synaptic connections. It is easy to modify network topology to realize new computing designs and applications due to wireless connectivity and learning by WPT.
- *Wireless MI system design:* A promising solution is proposed for the bottlenecks regarding on-chip communications and energy transfer by exploiting MI channels as discussed in [14] and [15] which becomes critical as neurons get smaller sizes. Wired and RF wireless alternatives have challenges for energy consumption, interfacing with the network, 3D design, achievable footprints, interference and frequency of operation. Although memristor architectures perfectly combine memory and computation tasks together, they have the same challenges for massive numbers of neurons, and energy consumptions in resistive synaptic changes and wiring resistances [10]. MI design eliminates complexity while achieving WPT with any neuron.
- *Scalability and flexibility:* Significantly large number of synaptic connections supporting arbitrary connection geometries of neurons, e.g., with randomly oriented coils and shapes, are proposed with flexible design of neuron. The number of synaptic connections in spherical geometries depends on the sizes of individual neurons and coils inside it in analogy with biological origin.
- *Robustness:* It has robustness to signaling errors, noise and interference due to learning by energy efficiency of SCs. Wireless connection and stand-alone design of each neuron allow for hardware errors or external impacts breaking the device. Healthy neurons after disintegration learn the new topology by energy transfer from neighbor neurons and continue to operate.
- *KHz to sub-THz synaptic speed*: Recent theoretical advancements of nanoscale coils in [14] allow sub-THz WPT compared with biological responses on the orders of milliseconds (sub-KHz) [20].
- *Large resolution synaptic weight capability*: Synaptic weights are implemented with modulated energy efficiencies rather than conductance values such as in memristors. Synaptic weight resolution by a parallel set of S coils includes 2^S levels by introducing a novel concept for weight adaptation by tuning WPT efficiency. It can further be improved with coil topology or MI metamaterials [23].
- *Allowing asynchronous operation*: MI system neglects signaling and synchronization problems but evaluates WPT efficiency adapting to unreliable properties of synaptic coil connections.
- *Practical applications for pattern recognition*: MI neuromorphic network modulating the energy flow by using switching, impedance matching and excitation voltage adaptation intrinsically allows to identify different patterns of energy transmission among the coils. The distribution of the power throughout the network with large number of coils allows to solve significantly large and complicated pattern recognition problems.

III. WPT BASED MI NEURON MODELING

The proposed neuron architecture includes four different coil groups, i.e., axon, dendrite, synaptic and soma cells labeled with the colors blue, black, green and red as shown in Fig. 1(a). 3D spherical architecture of a neuron is shown in Fig. 1(b) where the outer shell includes axon and dendrite coils as energy transmitting and receiving parts, respectively. Inner part includes multiple shells analogical to soma and nucleus for generating energy and distributing received energy among axon coils for the neighbor connections [19]. Coils are distributed on the shells of the neuron designed with respect to the specific application or in a uniform manner based on polyhedral structures, e.g., Goldberg polyhedrons. A Goldberg polyhedron is a convex polyhedron made from hexagons and pentagons denoted with the notation $GV(m, n)$ with $20\,T$ vertices, $30\,T$ edges, $10\,T+2$ faces consisting of 12 pentagons and $10\,(T-1)$ hexagons where $T = m^2 + m\,n + n^2$ [25]. An example of the coil topology with $m = 2$ and $n = 1$ is shown as the outer shell in Fig. 1(b). It has physical analogy in the topology of Carbon atom clusters such as fullerene (C_{60}) inspiring the proposed architecture. Furthermore, such structures are utilized for creating homogeneous magnetic field distributions in meta-material improved architectures [35]. A single neuron includes intra-neuron (axon, dendrite and soma) and synaptic WPT as modeled in detail in Section IV where the inter-coil relations are based on fully coupled MI model with (6) and (9), respectively. On the other hand, a single coil is considered as the smallest building block to implement a single neuron which can modulate the energy flow in the neighborhood as discussed in Section VII.

Energy is transmitted by using axon coils through synaptic coil channel forming a waveguide (WG) to the dendrite coils as shown in Fig. 1(a) with variable inter-coil distance between neighbor synaptic coils oriented in parallel. WGs are MI structures resulting in an adaptive energy transmission based on inter-coil distance, orientation, resonance frequency and coil properties [14], [15], [26]. In this article, a novel utilization of WGs is performed for synaptic connections with adaptive weight. The coils inside a neuron form a mutually coupled MI network such that the orientation and power levels in the coils of the inner shells, i.e., soma and nucleus coils, are adapted with respect to the received power levels from the dendrites. They achieve to organize the distribution of the received energy from the dendrites to the axons with varying level of balance among the axon coils. Energy is either distributed uniformly among the axon coils or in an unbalanced manner while satisfying a threshold received power level P_{th} to fire an equivalent amount of output power to the neighbor neuron. Redistribution of received energy by tuning both the generated soma energy and topology of soma coils, i.e., for realizing desired activation function, requires time and energy resources. However, efficiency is improved by limiting the topology adaptations for soma and synaptic coils to electrically achieved ON-OFF switching or mechanisms without switching but including only power modulation. Improving the speed of activation function is an open issue to realize an ultra-high speed MI neuromorphic computing architecture.

Signaling based action potential transmission and firing mechanisms control ion channels while each transmission on a synapse consumes energy during various chemical processes including vesicle transmission. Electrical signaling processes are the major consumer of Adenosine triphosphate (ATP) energy used in the brain with the major signaling energy use is on synaptic transmission [19]. ATP molecules are utilized per vesicle transmitted in the synapse while observing the effects of synapse strength on energy expenditure [19]. On the other hand, proposed architecture utilizes WPT based firing and integration mechanism inspired from activation potential based processes in nervous system. Coils transmit energy as a form of signaling while collecting the required energy from neighbor synapses with a fundamentally different operation architecture compared with signaling based artificial designs. Synaptic weight enhancement improves WPT efficiency for neighbor neurons. Therefore, WPT triggers the transmission to next neighbor neurons compared with action potentials triggering chemical events consuming energy in each neuron.

The proposed architecture is naturally energy harvesting, i.e., axon and synaptic coils receive energy while modulating the flow of energy with the loads denoted by Z_L and Z_s, respectively, as thoroughly modeled in Section IV for a given set-up of active voltage sources in the dendrite and soma coils and the given configuration of the network at the time interval t. It is assumed that dendrite and axon coils have the capability to perform both energy transmission and reception by adapting their circuit with a switch structure. For example, if the dendrite coil is determined to be fired and it has enough energy, then it can perform in the transmitting (Tx) mode. Similarly, it may not have enough energy to activate the voltage source and can harvest energy from the neighbor neurons by utilizing an energy harvesting load in the receiving (Rx) mode. The proposed universal circuit theoretical model in (1) and (2) in Section IV is valid for all WPT neuromorphic networks by assigning various roles to each coil. In fact, complicated geometries of coil geometries can be perceived as a neuromorphic hardware by considering each coil as a single neuron element. In this case, a coil is either consuming an active power with active voltage source or it harvests energy with an appropriate load. The coupling among the coils depending on the geometry and the current mode of each coil together determine the flow of energy throughout the network as a novel form of synaptic plasticity. Therefore, proposed architecture and modeling are not constrained to the polyhedral type neurons. An example is illustrated in Section VII where three consecutive layers of coil arrays are utilized for a pattern recognition problem.

A. NEUROMORPHIC WPT HARDWARE DESIGN

The coils in the proposed system design are targeted to be in nanoscale and microscale dimensions. Graphene or graphite based coil structures are future promising with important electrical, mechanical and geometrical advantages of graphene including atomic scale dimensions, high strength, high current capacity, planar structure, easy manufacturing, ultra-low weight and flexibility [14], [17], [27]. In this article, the coils are assumed to be realized by graphene structures with substrates reducing the substrate loss as thoroughly discussed in [14] and [27] such as utilizing thick quartz substrates as shown in Figs. 2(a), (b) and (c). The coils are made from graphene layers with the thickness of h and width w while having the coil radius of r. In addition, the coils are connected to a circuit for realizing energy harvesting, voltage source activation and switching. The design of the optimum hardware circuit for performing the functions is out of scope of the article. The geometry of the circuit is tuned for the specific application either as an on-chip structure as shown in Figs. 2(a) and (b) or with more space preserving geometry as shown in Fig. 2(c). All-graphene circuit architectures are promising to provide an all-in-one solution for future nanoscale system architectures while exploiting the advantages of graphene [14]. On the other hand, there are significant improvements in microscale and nanoscale circuit design such as utilizing graphene supercapacitors in energy harvesting and storage circuit [28], low power nanoscale switches with carbon nanotubes [29], THz electrical oscillation sources with resonant tunneling diode (RTD) monolithic microwave integrated circuits (MMICs) and high electron mobility transistors (HEMTs) [30], [31] or THz mechanical oscillators in the recent design by utilizing SMMs [24].

The networks of the neuromorphic WPT by utilizing the inductive coil circuits are shown in Figs. 2(d) and (e). In Fig. 2(d), coils units are attached on a polyhedral substrate

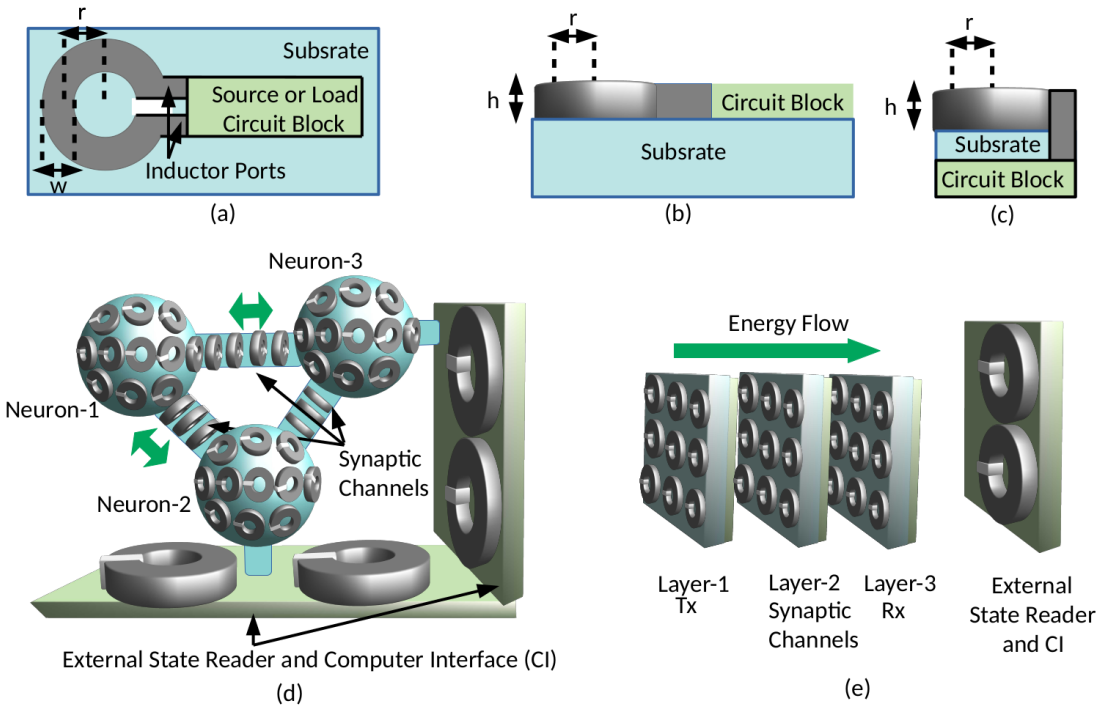

FIGURE 2. Hardware design of a single inductor coil and its circuit on the substrate with (a) top view, and (b) side view. The nanoscale/microscale inductor is connected to energy harvesting, switching and voltage generating circuit. (c) The geometry is optimized to reduce the area of the chip making it proportional to the coil area. (d) Neuromorphic network composed of three polyhedral neurons on the fixed structure of the substrate and the configuration of the external MI readers for the computer interface. (e) Layered neuromorphic WPT hardware with coil arrays on planar substrates designed for pattern recognition.

network with a fixed structure. The neurons and synaptic channels are implemented with coil and substrate combinations. There is an external hardware with MI coils to analyze and to read the state of the neuromorphic network, e.g., reading the adapted voltage levels, load impedance and harvested energy in each coil unit. It is necessary to provide a sub-unit for MI communications in the coil circuits to relay their state through the neuromorphic network to the external reader. Then, the state is stored and analyzed in external systems connected with a computer interface (CI) to the reader.

The number of neurons to be implemented in a volume of $1\,\text{mm}^3$ is numerically analyzed for neurons on Goldberg polyhedron outer shells of the type $GV(2,1)$ in Fig. 3 for varying coil radius r. It is assumed that each spherical neuron is placed in a cubic volume of $(\alpha_{sphere}\,2\,r\,R_e/r_0)^3$ where $\alpha_{sphere} = 1.1$ and $R_e = 175.7356\,\mu\text{m}$ for $r_0 = 30\,\mu\text{m}$ as simulated in Section VIII-C. It is observed that the number of neurons increases significantly as the experimentally implemented coil dimension decreases, e.g., reaching $\approx 10^6$ for $\approx 1\,\mu$m radius coils. On the other hand, the proposed neuromorphic WPT system is not constrained to specific neuron geometry. The fundamental design methodology is to modulate the energy flow which allows complicated coil geometries as a network of neurons where each coil is treated as a single neuron. In this case, the number of neuron units increases much more significantly as shown in Fig. 3 where it

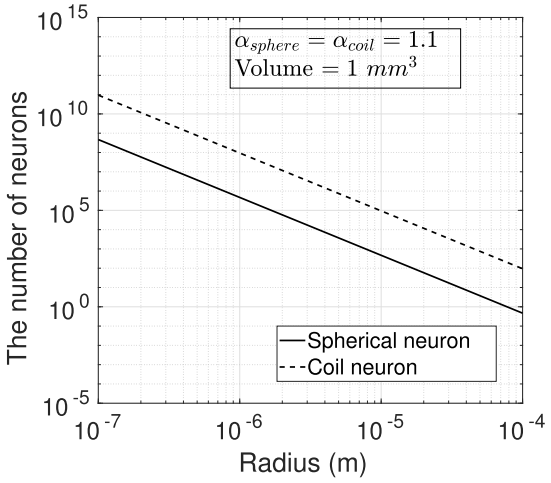

FIGURE 3. The total number of spherical neurons with Goldberg polyhedron geometry of $GV(2,1)$ and coil neurons with cubic volume of $(\alpha_{coil}\,2\,r)^3$ in a total volume of $1\ \text{mm}^3$ for varying coil radius r.

is assumed that a single coil is placed inside a cubic volume of $(\alpha_{coil}\,2\,r)^3$ and $\alpha_{coil} = \alpha_{sphere} = 1.1$. The number of neurons reaches $\approx 10^8$ for a coil radius of $1\,\mu$m as a highly promising amount for practical problems. The proposed numbers are comparable with the state-of-the-art implementations with different technologies on the orders of million neurons [32].

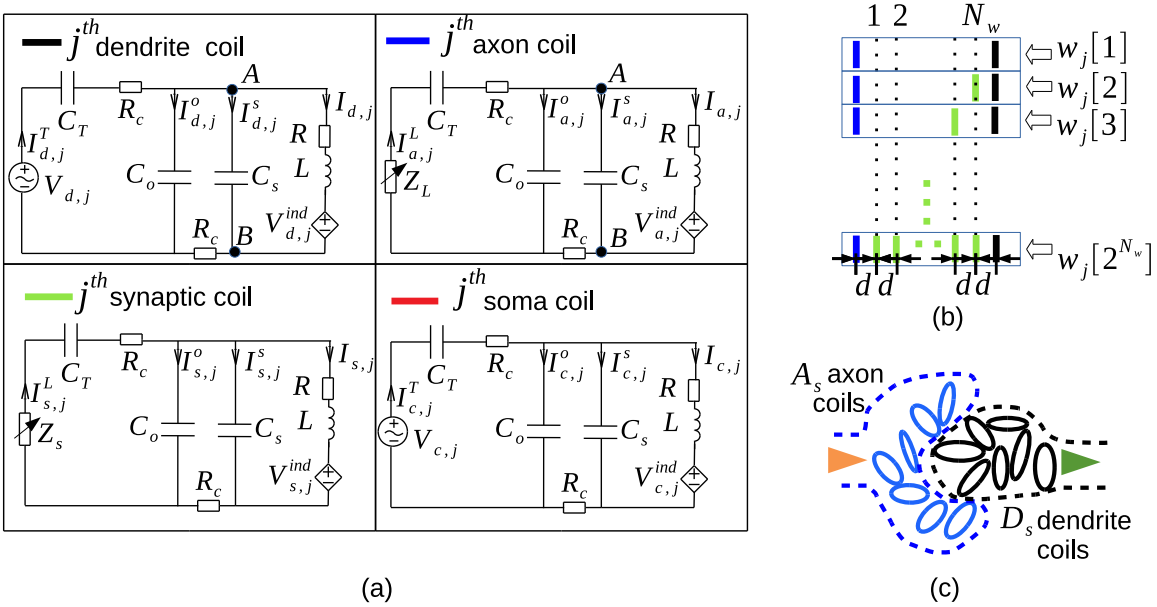

FIGURE 4. (a) Circuit theoretical equivalent model of each coil type as two-port RLC circuits with capacitance values of the substrate (C_s), overlap (C_o) and tuning (C_T), and contact resistance (R_c) where there is mutual inductance relationship among the coils in a MI network inducing voltages on each other. Synaptic coils include variable resistance Z_s tuning the channel. (b) SC modeling of jth dendrite where the weight is tuned by changing the topology and the number of active coils resulting in 2^{Nw} possible weight values in a single synaptic link, and (c) intertwined geometry of groups of axon and dendrite coils distributed and oriented randomly in 3D with a desired shape, e.g., analogical to biological origins.

In Fig. 2(e), a simpler hardware design is shown where coils are on planar substrates placed in parallel by treating each coil as a single neuron unit. The first layer has active voltage sources while the second and third layers have adaptive impedance. The second layer performs as a synaptic layer tuning the flow of energy to the third layer. The proposed structure is theoretically analyzed in Section VII and numerically simulated in Section VIII-D for the pattern recognition application. Next, topology of the coils is utilized in circuit theoretical modeling of the system performance.

IV. CIRCUIT THEORETICAL MODELING OF NEUROMORPHIC WPT NETWORK

Each coil is assumed to have identical two-port circuit theoretical model defined and experimentally implemented in various nanoscale and microscale inductor design studies [14], [17], [27] as shown in Fig. 4(a). The self impedance $Z_{self} = R + \imath L \omega$ includes the coil resistance R and the inductance L. It is assumed that substrate loss is eliminated with substrate materials such as thick quartz as realized for graphene or graphite inductors in [27]. The capacitive effects include the substrate (C_s), overlap (C_o) and tuning component (C_T) for the desired resonance frequency $\omega_0 = 2\pi f_0$. The voltage and current values in the following analysis denote the complex phasor representations [15], [26]. Self-resistance R and inductance L depend on ω especially for high frequencies and nanoscale sizes modeled and implemented for graphene inductors [14], [17]. In this article, it is assumed that the inductors are realized with graphene or graphite material modeled and experimentally implemented in detail for on-chip applications [17], [27]. Induced voltage on kth coil due to current I_l in lth coil is given by $\imath \omega M_{k,l} I_l$ where $\imath = \sqrt{-1}$ is the complex unity and $M_{k,l}$ is the mutual inductance between the coils [26].

Axon and synaptic coils in a single energy transmission across the neurons are modeled without any active voltage sources while dendrite and central soma coils are modeled with active voltage sources denoted by $V_{d,j}$ and $V_{c,j}$, respectively, where j is the index among the corresponding coil sets. Dendrite coils are assumed to have received energy from the neighbor neurons in previous transmissions and transmitting to the axons of the current neuron. The presented analysis is valid for both only a single neuron to analyze the implementation of nonlinear activation function mechanism and also for multiple neurons forming a complex neuromorphic WPT network. A single neuron analysis is provided to present the capability of implementing desired activation functions by tuning the neuron properties.

Axons and synapses are assumed to have varying receiver load impedance Z_L and Z_s, respectively, which are adapted for modulating energy transmission across the neuromorphic network. Induced voltage levels on jth axon, synapse, dendrite and soma coils are denoted by $V_{a,j}^{ind}$, $V_{s,j}^{ind}$, $V_{d,j}^{ind}$ and $V_{c,j}^{ind}$ while the currents on the inductor part are denoted by $I_{a,j}$, $I_{s,j}$, $I_{d,j}$ and $I_{c,j}$, respectively. The currents on the voltage sources of jth dendrite and soma coils are denoted by $I_{d,j}^T$ and $I_{c,j}^T$, respectively. The currents on the load of the jth axon coil and synapse are denoted by $I_{a,j}^L$ and $I_{s,j}^L$, respectively.

Assume that there are A_N, D_N, W_N and S_N number of coils in the neuromorphic network performing as axon, dendrite, synaptic channel and soma units, respectively, at the time interval indexed with t. The detailed circuit theoretical modeling of the circuits defined in Fig. 4(a) are provided in Appendix. The relation between voltage sources and currents satisfies the following:

$$\begin{bmatrix} \mathbf{V}_d(t) \\ \mathbf{V}_c(t) \\ \mathbf{0}_{A_N} \\ \mathbf{0}_{W_N} \end{bmatrix} = \mathbf{M} \begin{bmatrix} \mathbf{I}_d(t) \\ \mathbf{I}_c(t) \\ \mathbf{I}_a(t) \\ \mathbf{I}_s(t) \end{bmatrix} \tag{1}$$

where the mutual inductance matrix is defined as follows:

$$\mathbf{M} \equiv \begin{bmatrix} \mathbf{M}_{d,d}(t) & \mathbf{M}_{d,c}(t) & \mathbf{M}_{d,a}(t) & \mathbf{M}_{d,s}(t) \\ \mathbf{M}_{c,d}(t) & \mathbf{M}_{c,c}(t) & \mathbf{M}_{c,a}(t) & \mathbf{M}_{c,s}(t) \\ \mathbf{M}_{a,d}(t) & \mathbf{M}_{a,c}(t) & \mathbf{M}_{a,a}(t) & \mathbf{M}_{a,s}(t) \\ \mathbf{M}_{s,d}(t) & \mathbf{M}_{s,c}(t) & \mathbf{M}_{s,a}(t) & \mathbf{M}_{s,s}(t) \end{bmatrix} \tag{2}$$

and $\mathbf{0}_K$ is all zeros column vector of length K, the column vectors $\mathbf{V}_d(t)$, $\mathbf{V}_c(t)$, $\mathbf{I}_d(t)$, $\mathbf{I}_c(t)$, $\mathbf{I}_a(t)$ and $\mathbf{I}_s(t)$ are given by $\mathbf{V}_d(t) = \left[V_{d,1}(t) \dots V_{d,D_N}(t)\right]^T$, $\mathbf{V}_c(t) = \left[V_{c,1}(t) \dots V_{c,S_N}(t)\right]^T$, $\mathbf{I}_d(t) = \left[I_{d,1}(t) \dots I_{d,D_N}(t)\right]^T$, $\mathbf{I}_c(t) = \left[I_{c,1}(t) \dots I_{c,S_N}(t)\right]^T$, $\mathbf{I}_a(t) = \left[I_{a,1}(t) \dots I_{a,A_N}(t)\right]^T$, $\mathbf{I}_s(t) = \left[I_{s,1}(t) \dots I_{s,W_N}(t)\right]^T$, $\{.\}^T$ denotes transpose, and $\mathbf{M}_{s_1,s_2}(t)$ shows the mutual inductance coupling matrix among dendrite, soma, axon and synaptic coils where s_1 or s_2 denotes d, c, a or s. Circuit theoretical modeling presented in Appendix based on two-port model of the coils is utilized to calculate $\mathbf{M}_{s_1,s_2}(i,j;\,t)$ denoting the value at ith row and jth column of $\mathbf{M}_{s_1,s_2}(t)$ as follows:

$$\begin{cases} \iota\,\omega\,\dfrac{1-\Gamma_1}{\Gamma_2} M_{s_1,s_2}(i,j;\,t), & s_1 \neq s_2 \text{ and } (s_1 = d \text{ or } c) \\ \iota\,\omega\, M_{s_1,s_2}(i,j;\,t), & s_1 \neq s_2 \text{ and } (s_1 = a \text{ or } s) \\ \iota\,\omega\,\dfrac{1-\Gamma_1}{\Gamma_2} M_{s_1,s_1}(i,j;\,t), & (i \neq j) \text{ and } (s_1 = d \text{ or } c) \\ \iota\,\omega\, M_{s_1,s_1}(i,j;\,t), & (i \neq j) \text{ and } (s_1 = a \text{ or } s) \\ Z_{self} \,/\, \Gamma_2, & (s_1 = s_2 = d \text{ or } c) \text{ and } i = j \\ Z_{self} + \widetilde{Z}_L, & (s_1 = s_2 = a) \text{ and } i = j \\ Z_{self} + \widetilde{Z}_s, & (s_1 = s_2 = s) \text{ and } i = j \end{cases} \tag{3}$$

where Γ_1, Γ_2, $\widetilde{Z}_L$ and $\widetilde{Z}_s$ are defined in Appendix, $M_{s_1,s_2}(i,j;\,t)$ is the mutual inductance between ith coil of the set indexed with s_1 and jth coil of the set indexed with s_2 while $i \neq j$ for $s_1 = s_2$ and $M_{s,s}(i,j;\,t)$ is the mutual inductance between ith and jth coils of the set indexed with s. In some of the following discussions, we remove the time index t for simplifying the modeling.

Tx powers on jth dendrite and soma coil denoted by $P_{d,j}$ for $j \in \{1, 2, \dots, D_N\}$ and $P_{c,j}$ for $j \in \{1, 2, \dots, S_N\}$, respectively, become as follows [15], [26]:

$$P_{d,j} = \Re\{V_{d,j}^* I_{d,j}^T\} / 2; \quad P_{c,j} = \Re\{V_{c,j}^* I_{c,j}^T\} / 2 \tag{4}$$

where $I_{d,j}^T$ and $I_{c,j}^T$ denote the currents on the voltage sources as shown in Fig. 4(a). Rx power values in axon and synaptic coils of the neuron are expressed as follows [15], [26]:

$$P_{a,j} = |I_{a,j}^L|^2\, \Re\{Z_L\} / 2; \quad P_{s,j} = |I_{s,j}^L|^2\, \Re\{Z_s\} / 2 \tag{5}$$

On the other hand, the notations of $P_{T,j}(t)$ and $P_j(t)$ are used for the received and the transmitted power of the jth dendrite and the corresponding axon coils, respectively, when inter-neuron energy transfer occurs with synaptic channels as discussed in Section IV-B. In this case, the dendrite coil indexed with j is in the Rx mode and the corresponding axon coil in the neighbor neuron is in the Tx mode.

The model in (1) and (2) is valid for all neuromorphic WPT networks with complicated geometry and the assignments of dendrite, axon, synaptic and soma roles to the coils. These networks include neuron implementations without constraining to specific geometries, e.g., a single coil based neuron as discussed in Sections III and VII. Next, the models for a single neuron and synaptic channel isolated from the remaining network are presented to show the capabilities of performing nonlinear activation functions as discussed in Section V and for realizing synaptic plasticity with a high resolution.

A. SINGLE NEURON MODELING

A single neuron is isolated from the remaining network where it is assumed that dendrite coils transmit energy to the axon part of the neuron through the soma coil section of the neuron. The neuron is designed with unique geometrical structures including the polyhedral geometry shown in Figs. 1(b) and 2(d) having the dendrite and axon coils on the external shell while soma coils on the inner shell. Dendrite coils are assumed to have enough energy to activate the voltage sources while adapting the soma coil geometry and load impedance of the axon coil allows to implement desired non-linear activation functions as discussed in Section V. Assuming that a single neuron composed of D dendrite, A axon and S soma coils forms a coupled MI network, then the relation between voltage sources and currents at t satisfies the following in analogy with (1) by excluding the synaptic part:

$$\begin{bmatrix} \mathbf{V}_d(t) \\ \mathbf{V}_c(t) \\ \mathbf{0}_A \end{bmatrix} = \begin{bmatrix} \mathbf{M}_{d,d}(t) & \mathbf{M}_{d,c}(t) & \mathbf{M}_{d,a}(t) \\ \mathbf{M}_{c,d}(t) & \mathbf{M}_{c,c}(t) & \mathbf{M}_{c,a}(t) \\ \mathbf{M}_{a,d}(t) & \mathbf{M}_{a,c}(t) & \mathbf{M}_{a,a}(t) \end{bmatrix} \begin{bmatrix} \mathbf{I}_d(t) \\ \mathbf{I}_c(t) \\ \mathbf{I}_a(t) \end{bmatrix} \tag{6}$$

where the column vectors $\mathbf{V}_d(t)$, $\mathbf{V}_c(t)$, $\mathbf{I}_d(t)$, $\mathbf{I}_c(t)$, $\mathbf{I}_a(t)$ are given by $\mathbf{V}_d(t) = \left[V_{d,1}(t) \dots V_{d,D}(t)\right]^T$, $\mathbf{V}_c(t) = \left[V_{c,1}(t) \dots V_{c,S}(t)\right]^T$, $\mathbf{I}_d(t) = \left[I_{d,1}(t) \dots I_{d,D}(t)\right]^T$, $\mathbf{I}_c(t) = \left[I_{c,1}(t) \dots I_{c,S}(t)\right]^T$, $\mathbf{I}_a(t) = \left[I_{a,1}(t) \dots I_{a,A}(t)\right]^T$, and $\mathbf{M}_{s_1,s_2}(t)$ is the coupling matrix among dendrite, axon and soma coils where s_1 or s_2 denotes either a, d, or c. $\mathbf{M}_{s_1,s_2}(i,j;\,t)$ on ith row and jth column of $\mathbf{M}_{s_1,s_2}(t)$ satisfies the same equations in (3) while skipping the synaptic part. Next, SCs are analyzed circuit theoretically.

B. SINGLE SYNAPTIC CHANNEL MODELING

SC as shown in Fig. 1(a) is modeled in an isolated form from the remaining network where the power is transmitted

between the neighbor neurons. Assume that the power is transmitted from the axon of the neighbor neuron to the dendrite of the current neuron so that the dendrite coils will have energy to fire in the following time intervals. SC of jth dendrite is modeled as a WG [14], [26]. The distance between kth and $(k+1)$th coil equals to $d_{k,k+1}$ as shown in Fig. 1(a). If N_w coils are uniformly placed with inter-coil distance d for simplicity, then the received power in the jth dendrite coil of the neuron, i.e, $P_{T,j}(t)$, due to the transmitted power $P_j(t)$ from the axon coil of the neighbor neuron with the index $m \in \{1, 2, \ldots, A\}$ with the voltage level $V_j(t)$, is found by solving $\mathbf{V}_s(t) = \widetilde{\mathbf{M}}_j(t)\mathbf{I}_s(t)$. The voltage vector is $\mathbf{V}_s(t) \equiv [V_j(t)\ \mathbf{0}^T_{N_w+1}]^T$ and the current vector is $\mathbf{I}_s(t) \equiv [I^s_{a,m}(t)\ I_{s,1}(t)\ \ldots\ I_{s,N_w}(t)\ I^s_{d,j}(t)]^T$. $I^s_{a,m}(t)$ and $I^s_{d,j}(t)$ (adding a superscript s for SC) denote the transmitter current of the axon coil of the neighbor neuron and the receiver current of the jth dendrite coil of the current neuron, respectively. $\widetilde{\mathbf{M}}_j(k,l;t)$ equals to the following based on (3):

$$\begin{cases} \iota\,\omega\,\dfrac{1-\Gamma_1}{\Gamma_2}M_{|k-l|}(t), & k=1 \text{ and } l\neq 1 \\ \iota\,\omega\,M_{|k-l|}(t), & k\neq 1 \text{ and } k\neq l \\ Z_{self}\,/\,\Gamma_2, & k=l=1 \\ Z_{self}+\widetilde{Z}_s, & (k=l)\neq N_w+2 \text{ and } \neq 1 \\ Z_{self}+\widetilde{Z'}_L, & k=l=N_w+2 \end{cases} \tag{7}$$

where $\widetilde{Z'}_L$ is obtained from (54) in Appendix by replacing Z_L with Z'_L which is the load impedance of the dendrite coil at the end of the synaptic channel for harvesting energy, $M_{|k-l|}(t)$ is the mutual inductance between parallel coils of the indices k and l having the same central axis and the central distance of $(k-l)\times d$ [15], [26].

The weight of WPT based SC is modified by modulating Z_s or Z'_L. Coils are switched in the channel as ON-OFF by making $Z_s = 0$ or ∞ as shown in Fig. 4(b) leading to capability of generating 2^{N_w} different synaptic weights. Synaptic WG results in varying amounts of energy flow with a nonlinear dependence as shown in Section VIII-A. Novel nanoscale developments such as single molecule magnets, meminductors, metamaterials or combinations are promising to modulate the energy flow with high resolution, scalability and low resistive loss [14], [23], [24], [33].

Performance of WPT in the SC of the jth dendrite coil is defined by the synaptic weight indexed with $i \in \{1, 2, \ldots, 2^{N_w}\}$ as $w_j[i]$. It is calculated by finding $\widetilde{\mathbf{M}}_j[i]$ for each i with respect to the defined topology of the coils shown in Fig. 4(b) with the index i denoting topology not time. It is calculated as follows:

$$w_j[i] \equiv (|I^s_{d,j}[i]|^2\,\Re\{Z'_L\}\,/\,2)\,/\,P_j[i] \tag{8}$$

where index i is utilized as a functional variable for the parameters, $P_j[i] = \Re\{V^*_j[i]I^s_{a,m}[i]\}\,/\,2$ is the transmit power of the axon coil of the neighbor neuron with the index m and the voltage $V_j[i]$, and the numerator shows the received power by the dendrite coil. Next, a more flexible SC mechanism is introduced.

1) NON-SWITCHING SYNAPSE

Stable SCs with multiple axon coil entrance points are designed to diminish energy consumption due to switching and multiple resistive coils in the WG. In Fig. 4(c), randomly oriented sets of axon and dendrite coils are shown where the orientations can be set randomly by lowering the costs for design and manufacturing. Synaptic coils are replaced with randomly coupled and intertwined axon and dendrite coils as a novel form of SC implementation. Assume that the numbers of axon and dendrite coils corresponding to the synapse are given by A_s and D_s, respectively. The voltage vector in the axon group is denoted by $\mathbf{V}_a$ including the voltages V_{s_a} for $s_a \in \{1, 2, \ldots, A_s\}$. Current vectors in the axon and dendrite groups are denoted by $\mathbf{I}_a$ and $\mathbf{I}_d$ with current values I_{s_a} and I_{s_d} for $s_a \in \{1, 2, \ldots, A_s\}$ and $s_d \in \{1, 2, \ldots, D_s\}$, respectively. $\mathbf{M}_{int}$ denotes the mutual inductance matrix with fixed set of axon and dendrite coils in synapse with the size $(A_s+D_s)\times(A_s+D_s)$. Then, the following equation is satisfied for the synapse:

$$\begin{bmatrix}\mathbf{V}_a \\ \mathbf{0}_{D_s}\end{bmatrix} = \mathbf{M}_{int}\begin{bmatrix}\mathbf{I}_a \\ \mathbf{I}_d\end{bmatrix} \tag{9}$$

A set of higher energy coils is formed by choosing a subset of coils resonating approximately with the fixed voltage level denoted by V_0 and others close to zero voltage or with low energy behaving as passive coils. Then, there are 2^{A_s} different selections among A_s coils where each excitation vector type indexed with $\mathbf{V}_a[i]$ for $i \in \{1, 2, \ldots, 2^{A_s}\}$ results in a different set of currents in the dendrites with varying levels of total input power. Synaptic weight for each set of active coils is calculated by using the following:

$$w[i] \equiv \frac{\mathbf{I}^H_d[i]\,\mathbf{I}_d[i]\,\Re\{Z'_L\}}{\Re\{\mathbf{V}^H_a[i]\,\mathbf{I}_a[i]\}} \tag{10}$$

where $\{.\}^H$ denotes Hermitian and $\left[\mathbf{I}^T_a[i]\ \mathbf{I}^T_d[i]\right] = \left[\mathbf{V}^T_a[i]\ \mathbf{0}^T_{D_s}\right]\left(\mathbf{M}^{-1}_{int}\right)^T$.

The difference of the proposed system compared with the switched architecture is due to shifting the complexity and cost in weight adaption of synapses to the modulation of voltage levels in the sources. The voltage levels can be either adjusted by the source coil directly without any switching or switching the soma coils at the center of the neuron, e.g., by using network topology modulation method defined in [13] and [16]. Therefore, the synapses operate with high speed and lower power consumption. The objective becomes to minimize the energy consumption to adjust the voltage levels in the source coils either directly by the source coils or by switching of the soma coils to produce a non-volatile state distributing the energy to the desired set of source coils. Next, power dissipation modeling for the operation of a single neuron and SC transmission is presented.

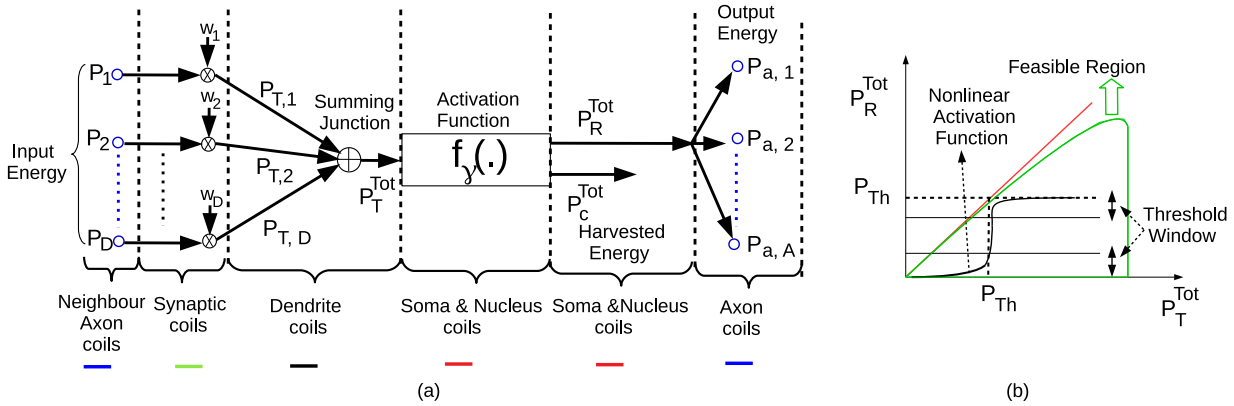

FIGURE 5. (a) Nonlinear modeling of MI neuron showing WPT across the neuron with input power received from the neighbor axon coils to the dendrite coils with synaptic weights w_j for $j \in \{1, 2, \ldots, D\}$ multiplying energy while distributing the received energy to the axon coils with the support of soma coils. (b) Nonlinear activation function $f_\gamma(.)$ implemented by using the set of feasible power levels.

C. POWER DISSIPATION OF SINGLE NEURON AND SYNAPTIC CHANNEL

Dissipated power in the system due to resistive components in the active sources and coils, and also switching or voltage adjustment mechanisms in SC or soma coils should be minimized. Consumed power through a single coil due to resistance R and contact resistances R_c is given as follows:

$$P_{x,j}^{-,res} \equiv |I_{x,j}|^2 R/2 + \sum_{i=1}^{2} |I_{x,j,i}^{c}|^2 R_c/2 \tag{11}$$

where $I_{x,j}$, $I_{x,j,1}^{c}$ and $I_{x,j,2}^{c}$ denote the currents passing through the coil resistance, the first and the second contact resistances shown in Fig. 4(a), respectively, and x refers to a, d, c or s denoting the axon, dendrite, soma or synaptic coils, respectively. $I_{x,j,1}^{c}$ is calculated as $I_{x,j}^{T}$ for x equal to d or c while it is calculated as $I_{x,j}^{L}$ for x equal to a or s as shown in Fig. 4(a) when the operation mode is such that dendrites transmit energy to the axons. In addition, $I_{x,j,2}^{c}$ is calculated as $I_{x,j} + I_{x,j}^{s}$ for all coil types. Furthermore, assume that $P_{x,j}^{-,V}$ denotes the energy consumed in a single coil due to the source component if it has active voltage source, i.e., operating in either mode for receiving and transmitting the energy. Total consumed power denoted by $P^{-,Tot}$ for the operation of a single neuron and the following synaptic transmission including switching or voltage level adjustment is as follows:

$$\begin{aligned} P^{-,Tot} = &\sum_{j=1}^{A} \left(P_{a,j}^{-,res} + P_{a,j}^{-,V}\right) + \sum_{j=1}^{S} \left(P_{c,j}^{-,res} + P_{c,j}^{-,V}\right) \\ &+ \sum_{j=1}^{D} (P_{d,j}^{-,res} + P_{d,j}^{-,V}) + \sum_{j=1}^{N_w} P_{s,j}^{-,res} \\ &+ P_{c}^{-,sw} + P_{s}^{-,sw} \end{aligned} \tag{12}$$

where $P_{c}^{-,sw}$ and $P_{s}^{-,sw}$ denote the power consumption values for the distribution of power through soma coils, e.g., by switching, and for adapting the synaptic weight in the SC either by switching or voltage level adjustment in the source coils, respectively. Energy consumption is found by multiplying with the cycle period T_p depending on the frequency of operation and application.

Consumed power in the coil resistances including axon and dendrite coils as defined in Section IV-B for a SC with the weight index i of jth dendrite coil satisfies the following:

$$P_{s,Tot}^{-,res}[i] / P_j[i] = 1 - w_j[i] \tag{13}$$

where the currents in some coils are zero depending on the weight index i as shown in Fig. 4(b) and the power is either transmitted to dendrite or dissipated through resistances in SC. As shown in Section VIII-A, improving $w_j[i]$ decreases resistive consumption by maximizing energy flow.

Advancements in 2D materials provide higher resistive performance compared with metallic structure [14], [17]. On the other hand, energy harvesting with resonating SMMs is proposed in [24] to generate non-contact voltage excitations. It is possible to utilize state-of-the-art mechanisms for electrical switching with minimum power consumption such as [29]. As discussed in Section IV-B1, various mechanisms are candidates to improve energy efficiency, e.g., voltage modulation without switching, and intertwined dendrite and axon coils without passive synaptic coils. Next, nonlinear modeling of neuron and activation function are presented with integrate-and-fire mechanism designed for energy.

V. NONLINEAR MODELING OF SINGLE NEURON AND WPT BASED ACTIVATION FUNCTION

Nonlinear modeling of sub-functions is shown in Fig. 5(a) for a single neuron. The numbers of dendrite and axon coils are denoted by D and A, respectively. It is analogical to the classical model including reception, summation, nonlinear activation and transmission to the neighbors [4]. Dendrite coils are connected to axon coils of the neighbors having the energies $P_1, P_2, \ldots, P_D$. The energy is transmitted through synaptic MI WGs resulting in decrease in the received power levels denoted by $P_{T,j} = w_j P_j$ for $j \in \{1, 2, \ldots, D\}$ where w_j is adapted by changing WG topology as discussed

in Section IV-B. Then, the total received power at the dendrites, which is to be transferred to the axon coils of the neuron, is given as follows:

$$P_T^{Tot} = \sum_{j=1}^{D} w_j P_j \equiv \sum_{j=1}^{D} P_{d,j} \tag{14}$$

The received power $\sum_{j=1}^{D} w_j P_j$ at the time interval t from the neighbor neuron is transmitted to the axon coils of the neuron at the next time interval with the Tx power levels $P_{d,j}$ for $j \in [1, D]$. On the other hand, flow of energy through multiple neurons at a single time step is also formulated and utilized as discussed in Section VII for pattern recognition.

Soma and center coils are adapted with respect to the set $\{P_{d,1}, P_{d,2}, \ldots, P_{d,D}\}$ where the desired nonlinear activation function $f_\gamma(.)$ is achieved. Output of the function which corresponds to the output energy is distributed among the axon coils with the power levels denoted by $P_{a,i}$ for $i \in \{1, 2, \ldots, A\}$. The activation function $f_\gamma(.)$ is chosen in the feasible region of input and output power values for a specific MI neuromorphic architecture as shown in Fig. 5(b). Various nonlinear formulations become possible such as distributing the received power with some proximity parameter $\gamma \leq 1$:

$$\sum_{i=1}^{A} P_{a,i} = f_\gamma(P_T^{Tot}) \tag{15}$$

where the following is satisfied for the distribution of the received energy among the axons:

$$\max_{i,j \in \{1,2,\ldots,A\}} \left\{ |P_{a,i} - P_{a,j}| \right\} / \left(\sum_{i=1}^{A} P_{a,i} / A \right) \leq \gamma \tag{16}$$

The value of $\gamma = 0$ achieves uniform distribution of power among axons analogical to the classical nonlinear model of integrate-and-fire mechanism [4]. The set of $\{P_{d,1}, P_{d,2}, \ldots, P_{d,D}\}$ for a given γ is required to be enlarged for robust activation depending only on the sum power rather than individual distribution of sum power among the dendrite coils. Soma coils are utilized for this task by adapting topology with ON-OFF switches and/or excitation voltage levels. The feasible region depends on the possible input and output power pairs which can be obtained with specified voltage levels and specific coil parameters. Threshold power P_{Th} is utilized for approximating the sigmoid function with specific windowing as shown in Fig. 5(b) while numerically analyzed in Section VIII-B where extensive numerical analysis is performed to realize adaptive feasible regions with respect to γ. The source coils, i.e., the dendrite coils, can be adjusted to be excited with the corresponding voltage levels after receiving the power in the previous time interval. Therefore, in the following sections which model the nonlinear activation mechanism, only a single time interval is analyzed where the dendrite coils transmit the target power.

Besides that, saturated high levels of input energy received from the dendrite coils are utilized to harvest energy in the soma coils in a different manner compared with the state of the art. The energy consumption is due to resistive elements in the coils, and adaptation and reorganization in soma and synaptic connections as discussed in Section IV-C. Energy efficiency is satisfied both in terms of WPT between neurons without any signaling complexity and also harvesting saturated energy received from dendrites. Saturated synapses with excess energy are utilized for energy harvesting firstly in the dendrite coils. In the next time interval, if all the received energy is transmitted, then energy harvesting occurs in the central soma coils for the case $P_{c,j} < 0$ when P_T^{Tot} is significantly high compared with P_{Th}. If P_T^{Tot} is barely larger than P_{Th}, then soma coils consume active power to carry received power to the axon coils since there is consumption in resistive elements and there is an internal distance between dendrites and axons inside the neuron cell reducing WPT efficiency. Increasing P_T^{Tot} reduces the required $P_{c,j}$ to have the desired total power in axons, i.e., P_{Th}. Next, the activation function is designed with the feasible input-output power pairs.

A. ACTIVATION FUNCTION DESIGN AND IMPLEMENTATION

Activation function is adapted based on the desired characteristics of the power distribution among the axon coils of the energy receiving neuron. $f_\gamma(.)$ is defined by specifying γ for output power distribution condition in (16) and nonlinear mapping between input P_T^{Tot} and output $P_R^{Tot} = f_\gamma(P_T^{Tot})$. For example, a sigmoid function gives zero output power for $P_T^{Tot} < P_{Th}$ and fires P_{Th} for $P_T^{Tot} \geq P_{Th}$. In the remaining discussions, $f_\gamma(.)$ is assumed to be the sigmoid function with P_{Th} for analogy with classical neuron models having integrate-and-fire mechanisms while the proposed model is valid for general nonlinear activation functions [4]. Then, an approximate activation function $\widehat{f}_\gamma(.)$ with the nonlinear mapping around activation threshold P_{Th}, e.g., satisfying a threshold window W_f around P_{Th} as shown in Fig. 5(b), is targeted for the neuron satisfying the following conditions:

$$\begin{cases} \leq W_f, & \text{if } P_T^{Tot} < P_{Th} \\ \geq (P_{Th} - W_f) \text{ and } \leq P_{Th}, & \text{if } \eta P_{Th} \geq P_T^{Tot} \geq P_{Th} \end{cases} \tag{17}$$

where $\eta \gg 1$ is some upper threshold for approximating the sigmoid function. Then, any set of input output pairs satisfying (17) is denoted by $\mathbf{P}_{T,R}^{Tot,f} = \{(P_T^{Tot}, P_R^{Tot});\ P_R^{Tot} = \widehat{f}_\gamma(P_T^{Tot})\}$. If the number of elements in $\mathbf{P}_{T,R}^{Tot,f}$ is increased and covers both sides of P_{Th}, then implemented activation function well approximates the desired activation function. Then, given $\widehat{f}_\gamma(.)$, the set of feasible input-output powers achievable in the neuron is denoted by the following:

$$\widehat{\mathbf{P}}_{T,R}^{f} \equiv \Bigg\{ (P_{d,1}, \ldots, P_{d,D}, P_{a,1}, \ldots, P_{a,A}); \left(\sum_{j=1}^{D} P_{d,j}, \sum_{k=1}^{A} P_{a,k} \right) \in \mathbf{P}_{T,R}^{Tot,f} \Bigg\} \tag{18}$$

The count of the elements in the set $\widehat{\mathbf{P}}_{T,R}^{f}$ is defined by N_f. Furthermore, a uniformity performance parameter

denoted by $\sigma_j^f(l)$ is defined for each dendrite coil where $j \in \{1, 2, \ldots, D\}$, $l \in [1, \eta P_{Th} / \Delta_P]$ along the intervals $(l-1)\Delta_P \leq P_T^{Tot} \leq l\Delta_P$. If $\sigma_j^f(l)$ is larger for the power interval l, then more robust realization of $f_\gamma(.)$ is achieved by covering different sets of input power distribution with the same total power. $\sigma_j^f(l)$ is defined as the standard deviation of $P_{d,j}(k)$ for varying index $k \in [1, N_f]$ in the feasible set $\widehat{\mathbf{P}}_{T,R}^f$ as follows while $\mu_j(l) \equiv \sum_{k=1}^{N_l} P_{d,j}(k) / N_l$:

$$\sigma_j^f(l) \equiv \sqrt{\frac{1}{N_l - 1} \sum_{k=1}^{N_l} |P_{d,j}(k) - \mu_j(l)|^2} \tag{19}$$

where N_l is the number of elements in $\widehat{\mathbf{P}}_{T,R}^f$ satisfying $(l-1)\Delta_P \leq P_T^{Tot} \leq l\Delta_P$.

On the other hand, performance metrics for a single realization index k in the feasible set are defined as follows:

$$\overline{\mu}_o(k) = \frac{1}{N_{coil}} \sum_{j=1}^{N_{coil}} P_{o,j}(k) \tag{20}$$

$$\overline{\sigma}_o(k) = \sqrt{\frac{1}{N_{coil} - 1} \sum_{j=1}^{N_{coil}} |P_{o,j}(k) - \mu_o(k)|^2} \tag{21}$$

where o refers to d, a and c and N_{coil} refers to D, A and S for the dendrite, axon and soma coils, respectively. This metric is more suitable to utilize for big neurons of polyhedron type with a large number of coils as simulated in Section VIII-C.

Feasible set is formed and analyzed by applying various combinations of excitation voltages (V_{exc}) to the dendrite and soma coils. It is also assumed that the soma coils are able to adjust their physical orientation by providing another dimension to modulate the flow of energy. Then, the sets of coil orientations and the voltage levels of excitation in the soma coils are denoted by $\mathbf{A}_c(i)$ for $i \in \{1, 2, \ldots, N_{\theta,\phi}\}$ and $\mathbf{V}_c(i)$ for $i \in \{1, 2, \ldots, N_v\}$, respectively. $\mathbf{A}_c(i)$ includes the group of specific orientations of S soma coils, i.e., $(\vec{n}_1, \vec{n}_2, \ldots, \vec{n}_S)$. $\mathbf{V}_c(i)$ includes a specific group of the voltage excitation among the soma coils with the values $(V_{c,1}, \ldots, V_{c,S})$. Then, there is total of $N_{\theta,\phi} \times N_v$ different configurations of soma coil system allowing to realize activation function. If it is assumed that voltage values for dendrite coils are in the set $V_{d,j} \in \{0, \Delta V_j, 2\Delta V_j, \ldots, V_j^{max}\}$ for $j \in \{1, 2, \ldots, D\}$, then the total number of WPT schemes (N_P) is given as follows:

$$N_P = N_{v_c} \times N_{\theta,\phi} \times \prod_{j=1}^{D} N_{v_j} \tag{22}$$

where $N_{v_j} \equiv (V_j^{max} / \Delta V_j + 1)$. All the input and output power levels do not satisfy $\widehat{\mathbf{P}}_{T,R}^f$ and a subset with N_f schemes is utilized to generate activation function. In Section VIII, a heuristic approach is utilized to realize a feasible set while an optimization framework maximizing N_f and $\sigma_j^f(l)$ by setting $\mathbf{A}_c$, $\mathbf{V}_c$, ΔV_j, V_j^{max} for each jth dendrite coil is an open issue. Next, a novel synaptic plasticity rule is defined based on the energy difference between neighbor neurons.

VI. ENERGY FLOW BASED SYNAPTIC PLASTICITY

Hebbian learning methods are throughly modeled in [4] where synaptic weight between two neurons denoted by w is adapted with Δw based on various rules where x_{pre} and x_{post} represent pre-synaptic and post-synaptic signals, and t_{pre} and t_{post} represent their timing, respectively. $\Delta t \equiv t_{post} - t_{pre}$ is the time difference of arrival of the synaptic events. Classical rules include (a) activity product rule with $\Delta w = \eta_a x_{pre} x_{post}$, (b) covariance hypothesis rule with $\Delta w = \eta_b (x_{pre} - \overline{x}_{pre})(x_{post} - \overline{x}_{post})$, and (c) spike timing dependent plasticity (STDP) of learning window with $\Delta w^{\pm} = \pm \eta_{c,\pm} e^{\mp \Delta t / \tau_\pm}$ having learning window sizes of τ_+ and τ_- and learning rates of η_a, η_b and $\eta_{c,\pm}$.

In the WPT based neuromorphic architecture, the rules are modified by replacing signals with transmitted energies and timing difference with the energy difference. Relative energy difference similar to relative time delay between two neurons is defined as follows:

$$\Delta P_{i,j}(t) = P_{R,i}^{Tot}(t) - P_{R,j}^{Tot}(t) \tag{23}$$

where ith and jth neurons are assumed as the pre-synaptic and post-synaptic neurons, respectively, and $P_{R,i}^{Tot}(t)$ and $P_{R,j}^{Tot}(t)$ denote their respective total received powers. Therefore, two neurons firing at the same time, i.e., having an output power larger than P_{Th}, will have small power difference. Synaptic weight denoted by $w_{i,j}(t+1)$ between ith and jth neurons at the time interval $t+1$ is modified as follows:

$$w_{i,j}(t+1) = w_{i,j}(t) + \Delta w_{i,j}(t) \tag{24}$$

while Hebbian learning methods for MI neuromorphic system modifying $\Delta w_{i,j}(t)$ are defined as follows:

$$\Delta w_{i,j}^a(t) \equiv \eta_a P_{R,j}^{Tot}(t) P_{R,i}^{Tot}(t) \tag{25}$$

$$\Delta w_{i,j}^b(t) \equiv \eta_b \Delta P_{R,j}^{Tot}(t) \Delta P_{R,i}^{Tot}(t) \tag{26}$$

$$\Delta w_{i,j}^c(t) \equiv \begin{cases} \eta_{c,+} e^{-\frac{\Delta P_{i,j}(t)}{P_+}}, & \Delta P_{i,j}(t) > 0 \\ -\eta_{c,-} e^{\frac{\Delta P_{i,j}(t)}{P_-}}, & \Delta P_{i,j}(t) \leq 0 \end{cases} \tag{27}$$

where $\Delta P_{R,k}^{Tot}(t) \equiv P_{R,k}^{Tot}(t) - \overline{P}_{R,k}^{Tot}(t)$ for kth neuron, P_+ and P_- are learning power windows, $\overline{P}_{R,k}^{Tot}(t)$ denotes the average power until the time t, and η_a, η_b, $\eta_{c,+}$, and $\eta_{c,-}$ denote learning rates for different methods. Furthermore, learning methods such as memory-based, reinforcement and unsupervised methods [4] are architectures to be performed on the MI neuromorphic system as open issues.

VII. WPT NETWORKS AND PATTERN RECOGNITION

Universal model proposed in (1) and (2) in Section IV is valid for all neuromorphic WPT networks without requiring a special design of neuron geometry. In this section, a simple multi-layer architecture is introduced by assuming each coil as a separate neuron unit. The multi-layered architecture is composed of arrays of coils as shown in Figs. 6(a) and (b) where the first layer transmits power (Layer-1) and the final layer (Layer-3) receives the energy in analogy to firing and

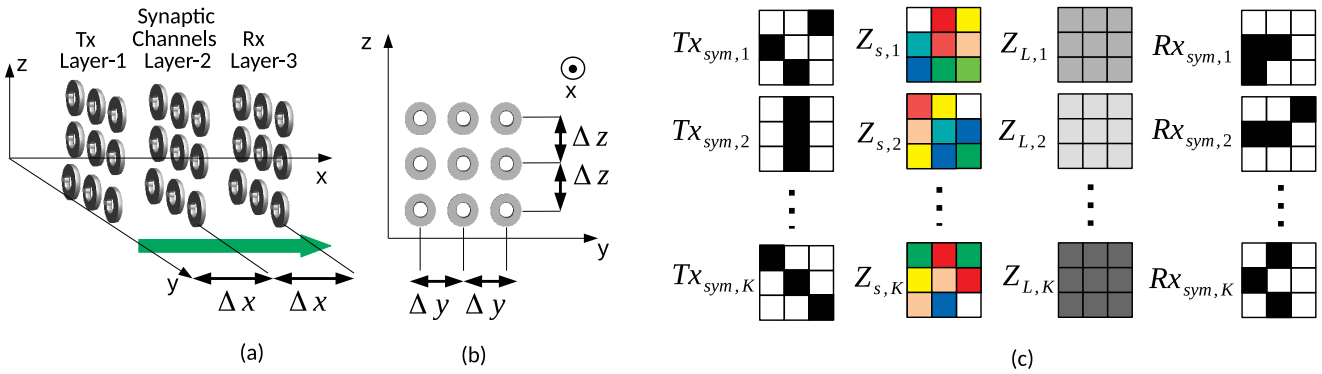

FIGURE 6. Three layer neuromorphic WPT network for pattern recognition with 3 × 3 array of coils on each parallel layer separated by Δx in x-axis, and (b) Δy and Δz in y-axis and z-axis, respectively. (c) K different Tx symbols with matched Rx symbols and synaptic weight adaptation with Z_s and Z_L in Layer-2 and Layer-3, respectively.

receiving neurons. The medium layer (Layer-2) is adapting synaptic weights among multiple neuron units, i.e., coils, modulating the energy flow direction and amplitude.

K different Tx symbols are shown in Fig. 6(c) where a symbol denoted by $\mathbf{Tx}_{sym,i}$ for $i \in [1, K]$ is formed by activating only a special subset of Layer-1 coils. Layer-2 and Layer-3 are assumed to be adapted with an energetic learning mechanism defined in Section VI by changing load impedance Z_s and Z_L, respectively, for each coil. If the target symbol is learned with repetitions and an appropriate learning mechanism is realized, then it becomes possible to discriminate each transmitted symbol by checking the received power distribution in Layer-3. For example, each symbol $\mathbf{Tx}_{sym,i}$ is mapped to a received symbol $\mathbf{Rx}_{sym,i}$ after an appropriate set of learning cycles with the adapted load impedance set $\mathbf{Z}_i$ including the impedance values of Layer-2 and Layer-3. Assume that $\mathbf{Tx}_{sym,i}$ and $\mathbf{Rx}_{sym,i}$ are matrices composed of ones and zeros corresponding to black and white boxes, respectively. The ones correspond to the foreground of the symbol while the zeros denote the background. Furthermore, assume that $\mathbf{V}_{Tx,i}$ corresponds to a unit voltage excitation in the respective black box positions in $\mathbf{Tx}_{sym,i}$ of Layer-1. The received power in Layer-3 is denoted with a matrix $\mathbf{P}_{Rx,i}$ as an array corresponding to the positional coordinates of the coils. Then, a power based correlation metric is defined as follows:

$$Corr(i,j) = P_{R,F}(i,j) - P_{R,B}(i,j) \tag{28}$$

$$= \mathbf{P}_{Rx,i} \odot \mathbf{Rx}_{sym,j} - \mathbf{P}_{Rx,i} \odot (1 - \mathbf{Rx}_{sym,j}) \tag{29}$$

$$= \mathbf{P}_{Rx,i} \odot (2\,\mathbf{Rx}_{sym,j} - 1) \tag{30}$$

where $\odot$ is the point-wise product between the matrices, $P_{R,F}(i,j) \equiv \mathbf{P}_{Rx,i} \odot \mathbf{Rx}_{sym,j}$ and $P_{R,B}(i,j) \equiv \mathbf{P}_{Rx,i} \odot (1 - \mathbf{Rx}_{sym,j})$ are the power levels received in the foreground and background of the matched reception symbol $\mathbf{Rx}_{sym,j}$, respectively, when the transmitted symbol is $\mathbf{Tx}_{sym,i}$ and the synaptic weight impedance is $\mathbf{Z}_i$. Observe that $\mathbf{Tx}_{sym,i}$ may not equal to $\mathbf{Rx}_{sym,i}$ and the target is to design a learning mechanism and a mapping between input-output pairs to maximize $Corr(i,j)$ when $j = i$. This is a simple example of pattern recognition mapping a specific Tx symbol to a unique load impedance and synaptic weight network to obtain a unique distribution of power in the receiver layer. In numerical simulation studies, an example is provided in Section VIII-D to match 3 × 3 patterns reliably.

VIII. NUMERICAL ANALYSIS

There are four different simulation scenarios implemented in this article denoted by Simul-A, B, C and D as follows:

- Simul-A: The synaptic channel with N_w centric coils in parallel and inter-coil distance of d in x-axis is simulated in terms of the effect of ON-OFF states of the coils and the load impedance at the receiver.
- Simul-B: The single neuron obtained with a simple geometry of the coils, i.e., in a circular orientation of the dendrite and axon coils and a single soma coil at the center with rotation capability, is simulated in terms of the non-linear activation function implementation.
- Simul-C: The single neuron obtained with Goldberg polyhedrons, i.e., axon, dendrite and soma coils on the surface of spherical shells, is simulated for implementing non-linear activation function.
- Simul-D: Layered neuromorphic WPT system is simulated for pattern recognition problem where three parallel layers containing arrays of coils are utilized to modulate the flow of energy from Layer-1 to Layer-3 by adapting the synaptic weight with Layer-2 and Layer-3 due to the impedance (Z_s and Z_L) variations.

Coil parameters used in simulation studies are shown in Table 2 while the simulation parameters for each scenario are listed in Table 3. The radius of the microscale coil is assumed to be $r = 30\,\mu$m while having the graphene layer width $w = 10\,\mu$m, the height $h = 30\,\mu$m and the number of turns as one for simplicity. The parameter values are based on graphene or graphite based modeling and implementations presented in literature studies, e.g., [27] where an implemented 3/4-turn inductor on quartz substrate has inductance of 0.34 nH, simulated resonance frequency of

TABLE 2. Coil parameters.

PARAM.	MEANING	VALUE
r	The coil radius	30 μm
w	Wire width	10 μm
h	Wire thickness (height)	30 μm
R	Coil resistance	0.2253 Ω
R_c	Contact resistance	0.1560 Ω
L	Coil inductance	2.94 pH
C_o	Overlap capacitance	0.2 fF
C_s	Substrate capacitance	2 fF
C_T	Tuning capacitance	0.26 pF
f_0	Resonance frequency	180 GHz

TABLE 3. Parameters for simulation scenarios.

SIMUL.	PARAM.	MEANING	VALUE
A	N_w	The number of synaptic coils	$\{2, 4, 6, 8, 10\}$
	V_{exc} (V)	Excitation voltage	1
	Z_L / R	Load impedance	1 to 10^3
	d	Inter-coil synaptic distance	$1.5 \times h$
B	D, A, S	The number of dendrite, axon and soma coils	3, 3, 1
	n_s	Outer shell index	1
	β	Coil placement ratio	1.5
	ϕ	Soma coil elevation angle	$\{0, \pi/10, 2\pi/10, \ldots, \pi\}$
	θ	Soma coil azimuth angle	$\{0, \pi/10, \ldots, 2\pi - \pi/10\}$
	P_{Th}	Threshold power	20 mW
	V_{exc} (V)	Excitation voltage	$\{0, 0.075, 0.15, \ldots 0.975\}$
	Z_L / R	Load impedance	10
	γ	Output power distribution	$\{0.1, 0.3, 0.5, 0.7\}$
	W_f	Power window	P_{Th} / 10
	ΔP	Power interval for $\sigma_j^f(l)$	P_{Th} / 128
C	D, A, S	The number of dendrite, axon and soma coils	36, 36, 32
	(m_e, n_e)	Goldberg polyhedron parameters for dendrite/axon shell	(2, 1)
	(m_i, n_i)	Goldberg polyhedron parameters for soma shell	(1, 1)
	R_e	Goldberg polyhedron radius for dendrite/axon shell	175.7356 μm
	R_i	Goldberg polyhedron radius for soma shell	105.8013 μm
	V_{exc} (V)	Excitation voltage	0 to 1
	N_{exc}	The number of random excitation voltage samples	5×10^4
	Z_L / R	Load impedance	$\{10, 10^2, 10^3, 10^4\}$
D	Δx	Inter-layer distance in x-axis	$1.5 \times h$
	Δy, Δz	Inter-coil distance in y and z axes	$2.1 \times \sqrt{r^2 + (h/2)^2}$
	K	The number of Tx symbols	63
	Z_s / R	Layer-2 load impedance	$\{0, 10^7\}$
	Z_L / R	Layer-3 load impedance	1 to 5000

$f_0 = 179$ GHz, the length of approximately 160 μm, the width of $w = 10\,\mu$m, thickness of $h = 260$ nm, $R = 26\,\Omega$, $R_c = 18\,\Omega$, overlap capacitance of $C_o \approx 0.2$ fF and the substrate capacitance of $C_s \approx 2$ fF. The proposed coil in this article has approximately the same length, i.e., $2\pi r \approx 188\,\mu$m, while having the thickness of $h = 30\,\mu$m much larger than the implemented example in order to decrease the resistance of the inductor. We assume that the coil resistance, contact resistance and the inductance scale with the thickness as $\propto 1/h$ for the same wire width w. Then, the proposed simulation parameters in Table 2 are obtained approximating the exact properties of the graphene inductor. The frequency is set to $f_0 = 180$ GHz with tuning capacitance C_T. The detailed circuit theoretical modeling of the coil circuit and the WPT network are provided in Appendix. More detailed experimental and simulation studies improve the accuracy of the proposed simulations while the proposed accuracy is high enough to analyze the fundamentals of WPT with graphene microscale coils. Thermal noise voltage $\sqrt{4\,\kappa_B\,T_r\,\Delta f\,(R + R_c)} \approx 3.3\,10^{-6}$ (V) is much smaller than the analyzed excitation voltage levels reaching one volt where $\kappa_B = 1.38 \times 10^{-23}$ J/K, $T_r = 300$ K and Δf is taken as f_0 / 100 for power transfer. The proposed system performance is limited by the efficiency of WPT and the power consumption in circuit components connected to the MI coils. These include many factors including resistive consumption, coil geometry, neuron size and inter-neuron distance, SNR and operation frequency. The performance of the system with nanoscale coils utilizing ultra-low power consumption and SNR is left as a future work.

Mutual inductance calculation is based on the general 3D modeling in [15] including position, arbitrary orientation and size dependency with detailed formulations. Experiments of the proposed WPT scenarios improve the accuracy of the mutual inductance calculations as an open issue while the experimented values can be inserted into the theoretical formulations without any change in the main formulation.

A. SIMUL-A: SYNAPTIC PLASTICITY

Synaptic weight adaptation is analyzed for varying N_w with inter-coil distance $d = 1.5 \times h$ for coupled neighbor synaptic coils as shown in Fig. 7(a). The physical length of link is given by $(N_w + 1)\,d$ while longer SCs are formed with increasing N_w. The maximum magnitude of the synaptic weight slightly decreases as N_w increases due to realizing a longer WG. The load impedance is set to $Z_L = 10\,R$ without optimization for analyzing the effect of ON-OFF states of the coils in the SC (Z_s in the coil is either 0 or ∞) on the synaptic weight as shown in Fig. 7(a). It is observed that the number of different weight values which can be assigned to the synaptic link increases to $\approx 10^3$ even with a small number of synaptic coils of $N_w = 10$. Therefore, ultra-sensitive weight adaptation is possible. On the other hand, the weight behaves nonlinearly with respect to different topologies of synaptic coils depending on mutual inductance matrix modeled in Section IV-B. SC promises high performance energy transmission by utilizing nanoscale/microscale coils and sub-THz frequencies as discussed in [14]. 3D SCs with ultra-sensitive weight adaptation and sub-THz energy transmission promise significant future applications.

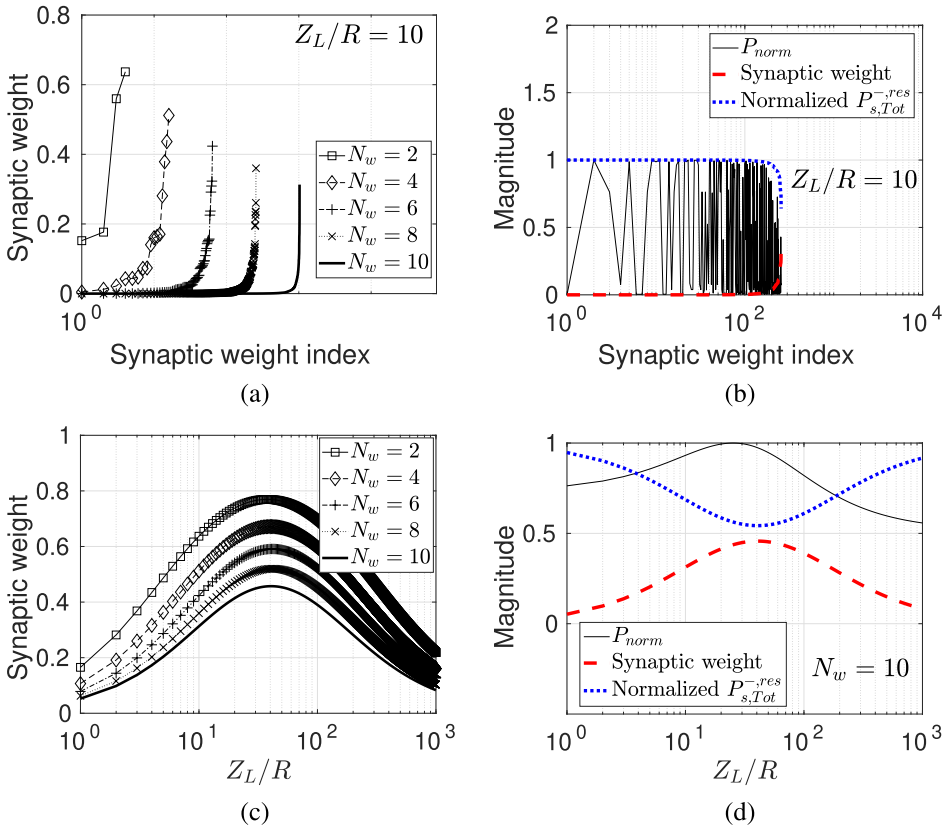

FIGURE 7. Simul-A: (a) Synaptic weight $w_j[i]$ for varying weight index $i \in \{1, 2, \ldots, 2^{N_W}\}$ and N_w, (b) magnitudes of normalized transmitted power (P_{norm}) from the axon of the neighbor coil, normalized power consumption ratio in resistive elements of coils ($P_{s,Tot}^{-,res}$) and synaptic weight for varying weight index where $N_W = 8$ and V_j is fixed. The effect of the load impedance Z_L on (c) the synaptic weight for varying N_w, and (d) P_{norm} and $P_{s,Tot}^{-,res}$.

In Fig. 7(b), the difference of the energy based and signaling based, e.g., voltage level based, synaptic transmissions are clearly shown. It is assumed that voltage excitation (V_{exc}) level in the dendrite coil is fixed to unity. The power transmitted from the axons of the neighbor coil (P_j) is normalized with $P_{norm}[i] = P_j[i] / \max_{i\in\{1,2,\ldots,2^{N_W}\}} P_j[i]$ where i is the index for the sorted synaptic weight $w[i]$. The total dissipated power in coil resistances, i.e., $P_{s,Tot}^{-,res}[i]$, is normalized leading to $P_{s,Tot}^{-,res}[i] / P_j[i] = 1 - w_j[i]$ for each index $i \in \{1, 2, \ldots, 2^{N_w}\}$ as shown in Fig. 7(b). Improving the synaptic weight reduces the resistive loss in the system. Therefore, efficiency of the system is improved by operating in high synaptic weight regime allowing energy flow efficiently through neurons. In the ideal case, lowest resistance system with adapted weights of SCs maximizes the energy efficiency of the system while performing neuromorphic computing successfully. It is observed that although the synaptic weight increases smoothly, the received voltage shows highly oscillatory and nonlinear behavior with significant difference between nearby levels in synaptic weight. The difference between magnitudes of the transmit power with similar synaptic weights can reach to the ratios of 10^3 leading to different behaviors between signaling and energy transmission based learning. The adaptation of synaptic weight can be coordinated with the amount of interference and noise in the synaptic link such that higher amount of power can be transmitted by only changing synaptic weight while fixing the transmission voltage level. The applied changes in synaptic weight require adaptation in input voltage levels to realize the transmission of the desired energy. The coupled behavior provides another optimization dimension, robustness and security to the effects of external noise and interference as an open issue and future work.

The effect of the load impedance Z_L is shown in Figs. 7(c) and (d). It is observed that the change of impedance provides another parameter to tune the synaptic weight with significant variations between $\approx$0 to $\approx$0.8 for $N_w = 2$ and between $\approx$0 to $\approx$0.45 for $N_w = 10$ as shown in Fig. 7(c). The load impedance not only changes the synaptic weight but also the transmitted power as shown in Fig. 7(d) requiring to analyze and to design the changes in the synaptic weight and energy flow simultaneously.

B. SIMUL-B: NONLINEAR ACTIVATION FUNCTION IN 2D GEOMETRICAL DESIGN OF NEURON

The implementation of nonlinear activation function is simulated with a simple neuron design having dendrite and axon coils around a circular shell indexed with n_s while having

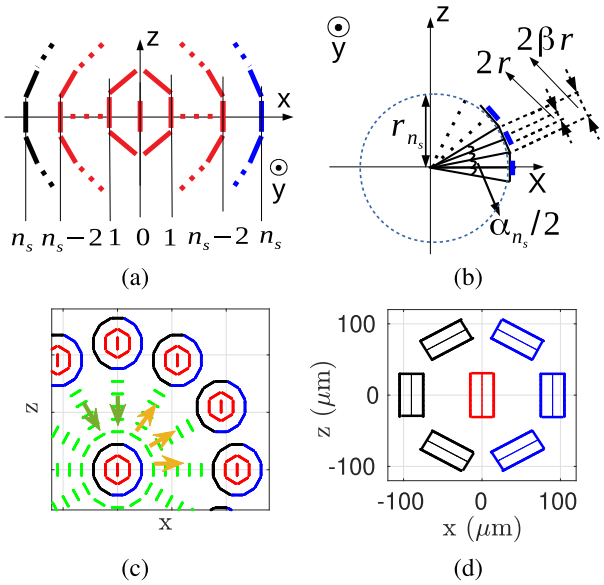

FIGURE 8. (a) Geometrical design of a neuron with the index of outer shell indexed with n_s, (b) placement of coils on the shell with the index n_s uniformly with angular separations α_{n_s}, (c) a single neuron receiving energy from multiple dendrites and transmitting energy to multiple synaptic waveguides by forming connections to multiple neighbor neurons, and (d) neuron geometry with single soma coil, three axon and dendrite coils where the thickness of the coils are shown with the radius $r = 30\,\mu$m and $h = 30\,\mu$m.

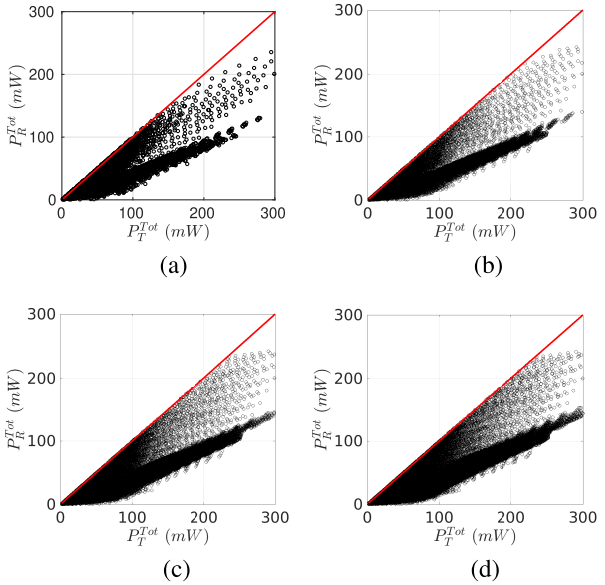

FIGURE 9. Feasible power sets for Simul-B (a) $\gamma = 0.1$, (b) $\gamma = 0.3$, (c) $\gamma = 0.5$, and (d) $\gamma = 0.7$.

soma coils on the inner shells and a freely rotating soma coil at the center modulating the flow of energy through the neuron as shown in Fig. 8(a). The shells are indexed with odd integers $1, 3, \ldots, n_s$ as shown Fig. 8(a). The radius of a single neuron is denoted by r_{n_s} while the index of the outer shell is given by some odd integer n_s. The even integers are not chosen to provide a symmetrical distribution of coils with respect to z-axis while more complicated geometries are possible without any limitation. The shells are symmetrically distributed with respect to the distance to the center. Outer shell includes both axon and dendrite coils while all the inner shells are of the type soma and nucleus. The proposed neuron structure is promising to be utilized to realize neuromorphic WPT network as shown in Fig. 8(c). A single neuron receives energy simultaneously from multiple neighbor neurons while transmitting the received energy simultaneously to the dendrite coils of multiple neighbors. The coil with the index j on ith shell for $i \in \{1, 3, \ldots, n_s\}$ is placed at the central position $Pos(i, j)$ corresponding to the following coordinate:

$$Pos(i,j) \equiv [x_{i,j} \quad y_{i,j} \quad z_{i,j}] = [r_i \cos(j\,\alpha_i) \quad 0 \quad r_i \sin(j\,\alpha_i)] \tag{31}$$

where coils (radius r) are placed on an area with radius $r_b = \beta\, r$ where $\beta > 1$ for reducing undesired interaction between closely separated coils. The coil placement ratio β shown in Fig. 8(b) is set to 1.5 in simulation studies which is enough to place thick coils reliably close to each other which can be optimized for tighter spatial volume. The radius r_i is set to $(i + 1)\, r_b$ while α_i is chosen as follows:

$$\alpha_i = 2 \arcsin\left(1 / (i + 1)\right) \tag{32}$$

which allows reliable sphere packing for spheres with radius r_b on a sphere with radius $(i + 1)\, r_b$ [34].

Axon and dendrite coils are assumed to have fixed orientation designed with respect to the required synaptic connections while the distribution of power with respect to γ is achieved by modulating soma topology, and excitation power levels in soma and dendrite coils. A group of soma coils placed in different orientations can be switched ON-OFF such as by utilizing electrical switching. It is assumed that each soma coil can have arbitrary orientation defined by azimuth (θ) and elevation angle (ϕ) in 3D such that in cartesian coordinates, normal vector of jth soma coil for $j \in \{1, 2, \ldots, S\}$ is given as follows [15] where the number of soma coils is denoted by S:

$$\vec{n}_j = \left[\cos(\theta)\, \sin(\phi) \quad \sin(\theta)\, \sin(\phi) \quad \cos(\phi)\right] \tag{33}$$

The outer shell index $n_s = 1$ is chosen for simplicity and as a proof of concept as shown in Fig. 8(d). It has three axon and dendrite coils, and a single soma coil with $D = A = 3$ and $S = 1$. The dendrite coils are indexed with Tx-1, Tx-2 and Tx-3. The excitation voltages for the dendrite and soma coils are chosen in the set $V_{exc} \in \{0, 0.075, 0.15, \ldots 0.975\}$ with $N_{v_j} = N_{v_c} = 14$ where $j \in [1, 3]$. The single soma coil is rotated to modulate the energy flow by orienting the soma coil in azimuth and elevation angles with increasing steps of π / 10 with $N_{\theta,\phi} = 20 \times 11$. The load impedance is set to $Z_L = 10 \times R$ for simplicity. N_P becomes $=14^4 \times 20 \times 11 \approx 8.45\, 10^6$.

The sets of input-output powers are simulated in Fig. 9 for varying γ increasing from 0.1 to 0.7. It is observed that

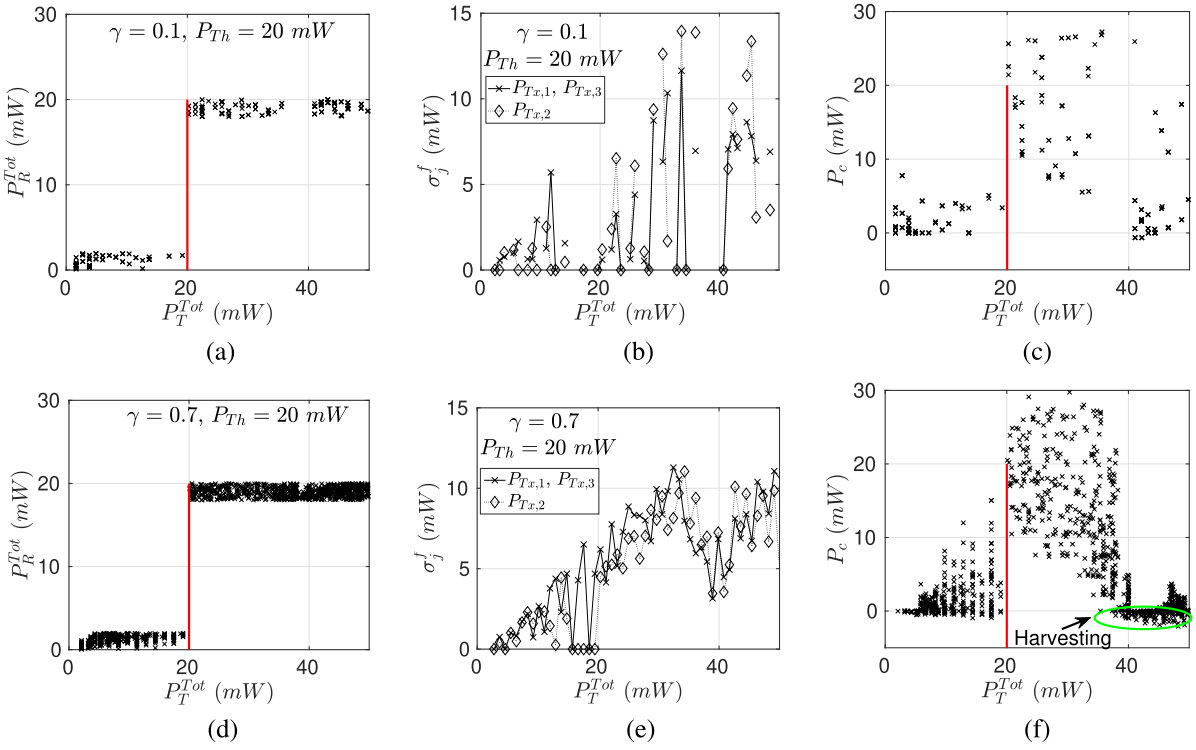

FIGURE 10. Simul-B with $\gamma = 0.1$ and $P_{Th} = 20$ mW where (a) activation function, (b) $\sigma_j^f(l)$ in power intervals of ΔP, and (c) P_c for varying input power P_{Tot}^T. The same performance parameters are simulated with $\gamma = 0.7$ for (d) activation function, (b) $\sigma_j^f(l)$, and (c) P_c for varying input power P_{Tot}^T.

relaxing the constraint of equivalent WPT among the axon coils increases N_f in the feasible set. Besides that, the set of pairs covers a large convex area under the curve $P_R^{Tot} = P_T^{Tot}$ allowing to implement varying functions, e.g., sigmoid function with firing threshold.

Activation function is analyzed within the thresholds of $\Delta P = P_{Th}/128$ while the feasible points are chosen with lower power consumption of soma coil (P_c) to improve the energy efficiency. In each interval, P_c is sorted and the lowest points are chosen if available. In Fig. 10(a), activation function is realized for $\gamma = 0.1$ with a windowing of $W_f = P_{Th}/10$ and $P_{Th} = 20$ mW. In Fig. 10(b), $\sigma_j^f(l)$ is analyzed where highly uniform distribution of input power is converted to the desired activation output as a robust system with the standard deviation on the orders of tens of mWs comparable with P_{Th}. In Fig. 10(c), the received power in the soma coil is shown. The performance is simulated in Figs. 10(d), (e) and (f) for $\gamma = 0.7$ with much more feasible points due to the relaxation in the received power distribution. It is observed that the consumed power is larger than P_{Th} in the proximity of $P_T^{Tot} \approx P_{Th}$ since there is a loss in the system due to positional distances and the resistive elements of the coils. However, as the input power is increased, soma coil requires smaller amount of energy to distribute the received power to the output by exploiting the higher received energy. If P_T^{Tot} becomes several times of P_{Th}, then soma coil does not consume a large power and the system efficiently distributes the power. Furthermore, after a critical level, soma coil starts to have the capability to harvest energy by experiencing negative power levels as shown in Fig. 10(f). In traditional neuron models, higher levels of activation voltages are not utilized for energy harvesting inside the neuron.

C. SIMUL-C: NONLINEAR ACTIVATION FUNCTION IN 3D POLYHEDRAL DESIGN OF NEURON

Neuron design with polyhedral geometry is implemented by using an outer shell of Goldberg polyhedron type $GV(2, 1)$ for axon and dendrite coils and an inner shell of the type $GV(1, 1)$ for the soma coils as shown in Figs. 11(a) and (b), respectively. The radii of the outer and inner shells are $R_e = 175.7536\,\mu$m and $R_i = 105.8013\,\mu$m, respectively. The total number of dendrite, axon and soma coils on a single neuron are $D = 36$, $A = 36$ and $S = 32$, respectively. The excitation voltages (V_{exc}) for the 36 dendrite and 32 soma coils are set between 0 and 1 in an independent and uniformly distributed manner with a total of $N_{exc} = 5 \times 10^4$ different random configurations to simulate the feasible performance parameters for the non-linear activation function. The energy flow is modulated with the change in load impedance of the axon coils in the set $Z_L/R \in \{1,\ 10,\ 10^2,\ 10^3\}$ compared with the rotation of the soma coil in Simul-B. Therefore, the energy flow depends only the excitation voltage distribution and the

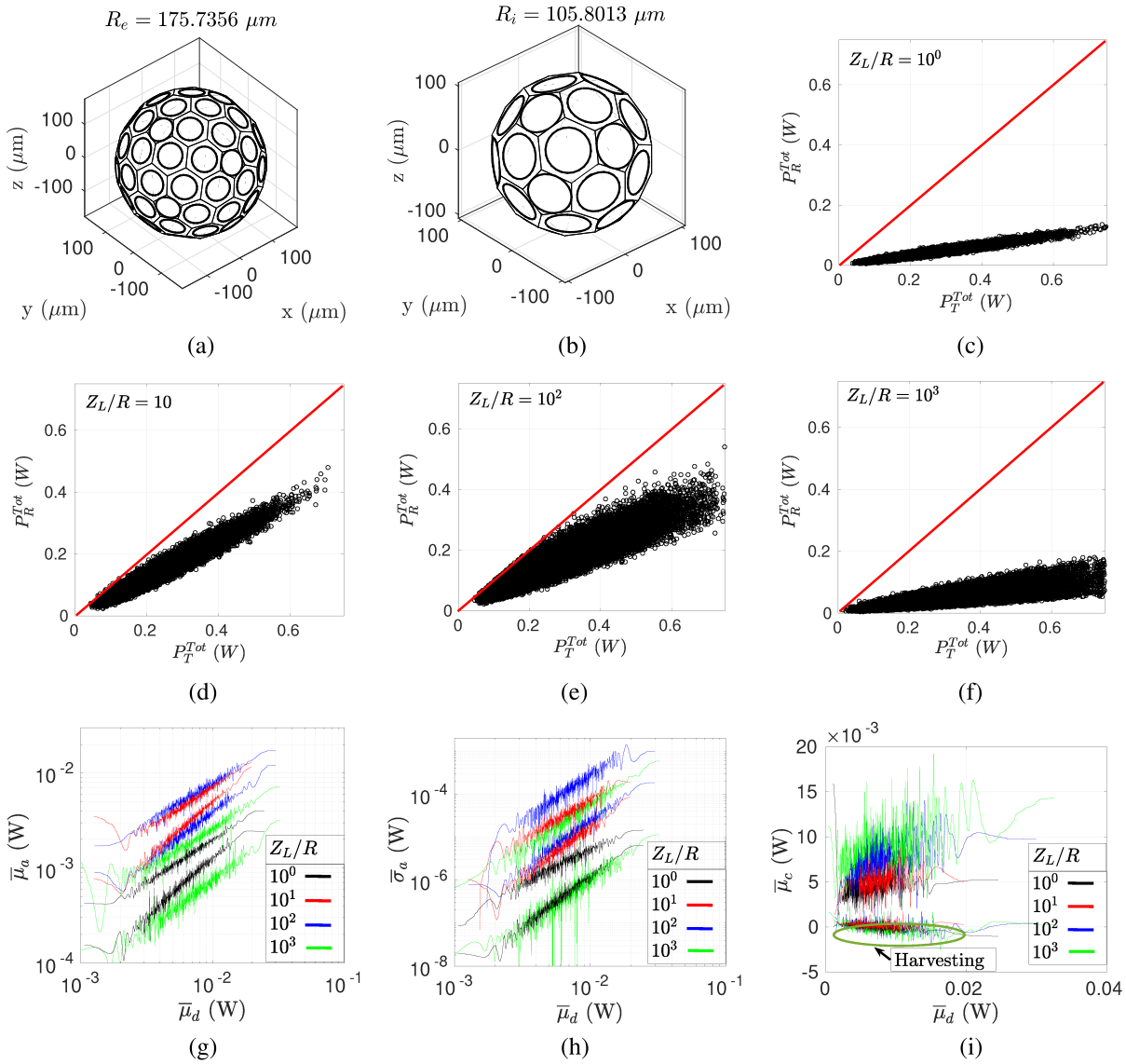

FIGURE 11. Simul-C: Goldberg polyhedrons for (a) the outer (the type $GV(2,1)$ polyhedron) and (b) the inner (the type $GV(1,1)$ polyhedron) shells to place the axon/dendrite and soma coils, respectively. The feasible set of input and output power levels for varying Z_L/R of (c) 1, (d) 10, (e) 10^2 and (f) 10^3. The upper and lower bound envelopes of (g) the variance and (h) the mean of the received axon power among the axon coils for each random excitation sample set for varying mean dendrite power. (i) The upper and lower bound envelopes of the mean transmitted power in soma coils for varying mean dendrite power.

load impedance. The feasible set of input-output total power levels for varying Z_L are shown in Figs. 11(c), (d), (e) and (f). It is observed that Z_L changes the feasible set with an optimum value maximizing the set for realizing the desired non-linear activation function. The largest feasible area is obtained for Z_L / 10^2 as shown in Fig. 11(e). The mean and the variance of the received axon power defined for each random excitation sample in (20) and (21) in Section V-A are shown in Figs. 11(g) and (h). There are two different envelopes with the same color for each Z_L corresponding to the upper and lower bounds of the obtained data. It is observed that a large variation in mean axon power is obtained with varying random excitation voltage levels while the corresponding variance among the power levels in the axon coils can be set to significantly minimum values compared with the mean. In other words, there are specific excitation sets satisfying a uniform distribution of a desired received power level throughout the axon coils. Therefore, targeted non-linear activation functions can be designed in the same manner with Simul-B. It is also observed that the soma coil power transmission covers a diverge area as shown in Fig. 11(i) even reaching to the energy harvesting regime.

D. SIMUL-D: PATTERN RECOGNITION WITH NEUROMORPHIC WPT LAYERS

Neuromorphic WPT network described in Section VII is simulated for pattern recognition. Three parallel layers of 3×3 coil arrays are utilized as shown in Fig. 12(a) showing

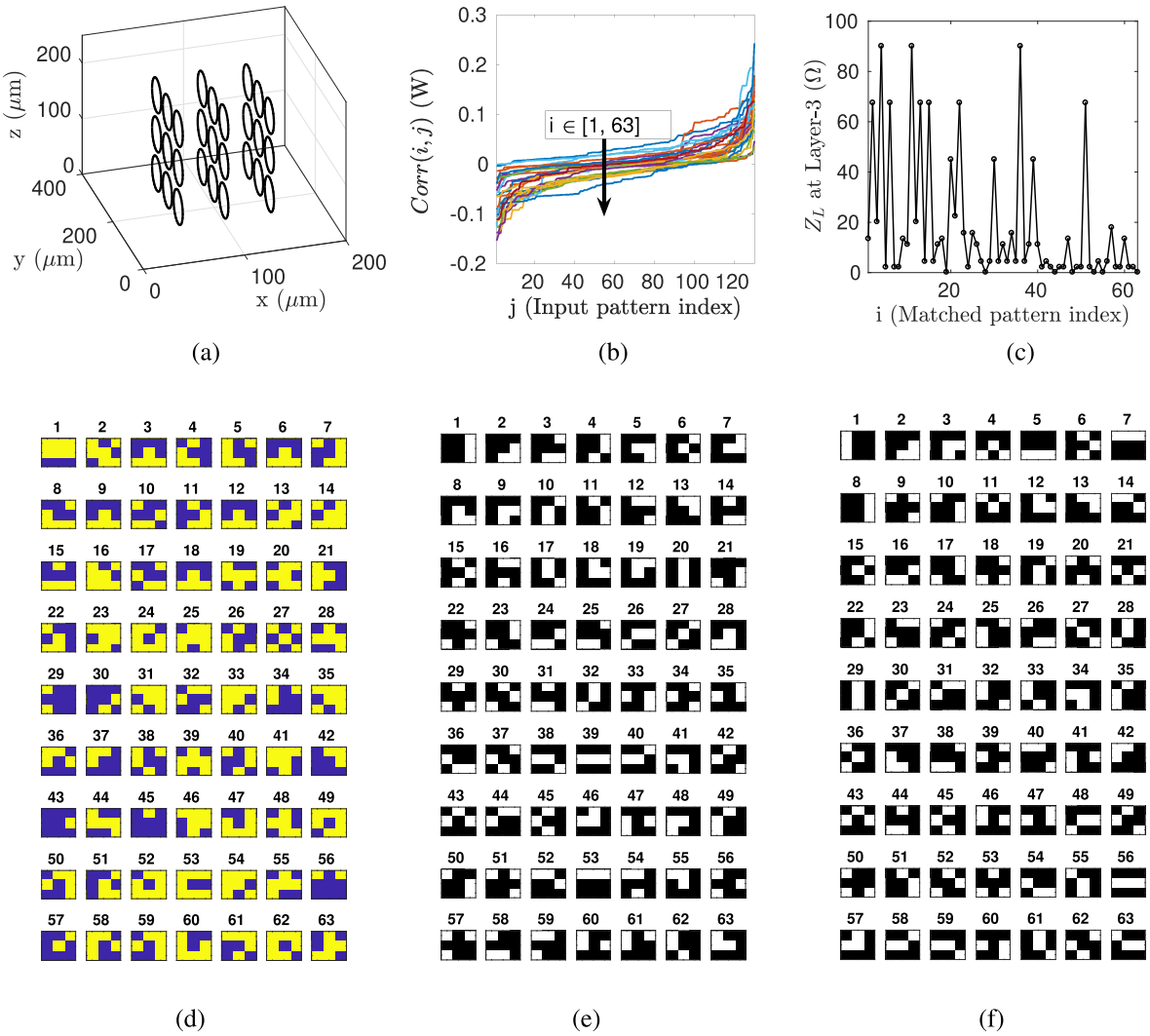

FIGURE 12. Simul-D: Layered neuromorphic WPT network for the pattern recognition where (a) the positions and the orientations of the central axes of the coils are shown. (b) The correlation for each Tx symbol $\mathbf{Tx}_{sym,i}$ for $i \in [1, 63]$ with reception symbol family $\mathbf{Rx}_{sym,j}$ for $j \in [1, 130]$ sorted for each i independently. Adapted (c) Z_L at Layer-3 and (d) Z_S at Layer-2 for each $i \in [1, 63]$. In (d), Z_S is either zero (blue) or $10^7 \times R$ (yellow) denoting the ON and OFF cases of the layers, respectively. The matched family of the symbols (e) $\mathbf{Tx}_{sym,i}$ and (f) $\mathbf{Rx}_{sym,i}$ giving the highest correlation in a uniquely identifiable manner.

the central axes of the coils. 3D illustration of the system showing the thickness of the coils is shown in Fig. 2(e). The distance between the layers is set to $\Delta x = 1.5 \times h$ due to the thickness constraint of the coils between the central positions of the layers. On the other hand, the central distance between the neighbor coils is set to $\Delta y = \Delta z$ calculated as $2.1 \max\{r, h/2, \sqrt{r^2 + (h/2)^2}\}$ in order to reliably prevent the coils from touching each other.

It is assumed that only three Tx coils are excited with unity voltage $V_{exc} = 1$ representing the symbols $\mathbf{Tx}_{sym,i}$ of Layer-1. There are $\binom{9}{3} = 84$ different possible input symbols. It is assumed that the receiver correlates the received power symbol with all the combinations of symbol matrices $\mathbf{Rx}_{sym,j}$ having three, two, one and zero coil excitation out of nine coils in order to identify the effect of noise and interference on the output where having less power compared with the transmitted symbol. In other words, the receiver correlates the received symbol with $\binom{9}{3} + \binom{9}{2} + \binom{9}{1} + 1 = 130$ different $\mathbf{Rx}_{sym,j}$ reception matrices and chooses the one with the largest correlation as the estimated Tx symbol. On the other hand, observe that the training phase is realized by matching each input symbol $\mathbf{Tx}_{sym,i}$ for $i \in [1, 84]$ with $\mathbf{Rx}_{sym,j}$ for $j \in [1, 130]$ providing the maximum $Corr(i, j)$. The training results in variations in the Layer-2 impedance values Z_s and the Layer-3 load Z_L. It is observed that only 63 different input symbols can be matched with the receiver symbols in a reliable manner, i.e., giving the maximum correlation for a uniquely identifiable (i, j) pair. The resulting correlation values for each 63 different $\mathbf{Tx}_{sym,i}$ with the all reception symbol family $\mathbf{Rx}_{sym,j}$ for $j \in [1, 130]$ are shown in Fig. 12(b). The correlation values are sorted for each input symbol i separately while plotted on the same figure where

the highest value corresponds to the matched reception symbol $\mathbf{Rx}_{sym,i}$. The uniquely identifiable set of input $\mathbf{Tx}_{sym,i}$ and reception symbols $\mathbf{Rx}_{sym,i}$ for $i \in [1, 63]$ are shown in Figs. 12(e) and (f), respectively, while the adapted set of Z_L values (uniform for Layer-3) and Z_s values (non-uniform for Layer-2) are shown in Figs. 12(c) and (d), respectively. The learning process is assumed to be realized with the methods defined in Section VI as a future work to optimize the methods in terms of the speed and performance for a target problem.

IX. OPEN ISSUES AND EXPERIMENTAL CHALLENGES

There is a set of experimental challenges and theoretical open issues to realize the prototype operating with massive numbers of neurons and to further extend the system design for higher performance.

- Design and experimental implementation of a complete neuromorphic architecture including energy harvesting, switching and voltage generating circuits shown in Figs. 2(a) and (b).
- Experimental implementations of large numbers of nanoscale/microscale coils on the substrates with the desired neuromorphic networking geometry with high coupling and operating in THz frequency by utilizing multi-layer graphene [14], [17], [27].
- Experimental implementation of energy consumption per synaptic energy transfer throughout the WPT network as discussed in Section IV-C depending on the coil properties, circuit implementations, network and neuron coil topology, switching mechanism and the features of voltage sources.
- Designing novel SC and neuron geometry, and learning algorithms performing based on energy transfer.
- Improvement and experimental implementation of pattern recognition solution proposed in the article for more complex problems with novel WPT based learning algorithms compared with similar architectures such as unsupervised learning and deep learning [36], [37].

X. CONCLUSION

In this article, WPT based modeling and analysis of neuron components and synaptic channels are proposed as a brain inspired neuromorphic design by exploiting MI networking and architecture. It promises solutions for the bottlenecks regarding the integration of communication, memory, computation and energy transfer. Numerical analyses provided for simple neuron geometries and synaptic channels with graphene coils achieve to perform fundamental functionalities of synaptic channel adaptation and nonlinear activation function mechanisms. Layered neuromorphic WPT network is designed and simulated for practical pattern recognition problems. The proposed architecture is intrinsically energy efficient while it has scalability, 3D integration and flexibility with wireless communications among neurons, robustness to physical failures, sub-THz operation frequency, a framework for exploiting nanoscale materials such as graphene, and maximum energy flow targeting minimum resistive components as a system design principle.

APPENDIX
CIRCUIT THEORETICAL MODELING

The equivalent impedance (Z_{eq}) of the circuit in Fig. 4(a) where $V_{d,j}$ is connected is given as follows:

$$R_c + \frac{1}{\imath\, C_T\, \omega} + \frac{1}{\imath\, C_o\, \omega + \left(R_c + \frac{1}{\imath\, C_s\, \omega + Z_{self}^{-1}}\right)^{-1}} \tag{34}$$

where $Z_{self} = R + \imath\, L\, \omega$. The resonance frequency ω_0 making the imaginary part zero is found as the solution of the following equation after a simple set of calculations:

$$E_{eq}\, \omega^6 + F_{eq}\, \omega^4 + G_{eq}\, \omega^2 + H_{eq} = 0 \tag{35}$$

where the following variables are defined:

$$E_{eq} = -C_o\, C_T\, C_s^2\, L^2\, R_c^2\, (C_o + C_T) \tag{36}$$

$$\begin{aligned} F_{eq} = {} & C_T \left(- C_o\, C_s^2\, R_c^2\, R^2\, (C_o + C_T) \right. \\ & + L^2\, (-C_o - C_s)\, (C_o + C_T + C_s) \\ & \left. + 2\, C_o\, C_s\, L\, R_c^2 (C_o + C_T) \right) \end{aligned} \tag{37}$$

$$\begin{aligned} G_{eq} = {} & C_T \left(R^2\, (-C_o - C_s)(C_o + C_T + C_s) \right. \\ & - C_o\, R_c^2\, (C_o + C_T) - 2\, C_o\, R_c\, R\, (C_o + C_T) \\ & \left. + 2\, C_o\, L + C_T\, L + 2\, C_s\, L \right) \end{aligned} \tag{38}$$

$$H_{eq} = -C_T \tag{39}$$

Dendrite coil circuits including active voltage source satisfy the following set of Kirchhoff equations:

$$-\frac{I_{d,j}^s}{\imath\, C_s\, \omega} + I_{d,j} Z_{self} + V_{d,j}^{ind} = 0 \tag{40}$$

$$-\frac{I_{d,j}^o}{\imath\, C_o\, \omega} + \frac{I_{d,j}^s}{\imath\, C_s\, \omega} + R_c (I_{d,j} + I_{d,j}^s) = 0 \tag{41}$$

$$\left(R_c + \frac{1}{\imath\, C_T\, \omega} \right) I_{d,j}^T + \frac{I_{d,j}^o}{\imath\, C_o\, \omega} - V_{d,j} = 0 \tag{42}$$

$$V_{\mathrm{AB}} - \frac{I_{d,j}^s}{\imath\, C_s\, \omega} = 0 \tag{43}$$

where $V_{AB} = \widetilde{V}_{d,j}$ is the complex voltage between the circuit nodes A and B and $I_{d,j}^T \equiv I_{d,j} + I_{d,j}^o + I_{d,j}^s$. The following is obtained by using (40-43):

$$V_{d,j} = \frac{1 - \Gamma_1}{\Gamma_2}\, V_{d,j}^{ind} + I_{d,j}\, \frac{Z_{self}}{\Gamma_2} \tag{44}$$

where Γ_1 and Γ_2 are defined as follows:

$$\Gamma_1 = \frac{1 + R_c\, \omega \big(- C_o\, C_T R_c\, \omega + \imath (C_o + 2\, C_T) \big)}{1 + \omega\, \left(\imath\, \xi_3 + \xi_5 - 2\, \imath\, \xi_4\, \omega^2 - \xi_2\, \omega \right)} \tag{45}$$

$$\Gamma_2 = \frac{\imath\, C_T\, \omega\, Z_{self}}{1 + \omega \left(\imath\, \xi_3 + \xi_5 - 2\, \imath\, \xi_4\, \omega^2 - \xi_2\, \omega \right)} \tag{46}$$

and $\xi_1 \equiv -\imath\, \omega\, (C_s\, R_c\, R + L) + C_s\, L\, R_c\, \omega^2 - R_c - R$, $\xi_2 \equiv L\, (C_T + C_s) + 2\, C_T\, C_s\, R_c\, R$, $\xi_3 \equiv R\, (C_T + C_s) + 2\, C_T\, R_c$,

$\xi_4 \equiv C_T\, C_s\, L\, R_c$ and $\xi_5 \equiv C_o\, \xi_1\, (C_T\, R_c\, \omega - \imath)$. The currents $I_{d,j}$, $I^o_{d,j}$ and $I^s_{d,j}$ are found as follows:

$$I_{d,j} = \frac{\imath\, C_s\, V^{ind}_{d,j}\, \omega - I^s_{d,j}}{C_s\, \omega\, (L\, \omega - \imath\, R)} \tag{47}$$

$$I^o_{d,j} = \frac{-\imath\, C_o\, C_s\, V^{ind}_{d,j}\, R_c\, \omega + I^s_{d,j}\, \xi_7}{C_s\, Z_{self}} \tag{48}$$

$$I^s_{d,j} = \frac{C_s\, \omega^2\, \left(V^{ind}_{d,j}\, \xi_6 / (\imath\, \omega) - C_T\, V_{d,j}\, Z_{self}\right)}{1 + \omega\, \left(\imath\, \xi_3 + \xi_5 - 2\, \imath\, \xi_4\, \omega^2 - \xi_2\, \omega\right)} \tag{49}$$

where $\xi_6 \equiv -1 + R_c\, \omega (C_o\, C_T\, R_c\, \omega - \imath (C_o + 2\, C_T))$ and $\xi_7 \equiv C_o\, \left(\imath\, \omega (C_s\, R_c\, R + L) - C_s\, L\, R_c\, \omega^2 + R_c + R\right)$.

Similarly, circuit theoretical equations for the axon coils are calculated as follows by using the models in Fig. 4(a):

$$-\frac{I^s_{a,j}}{\imath\, C_s\, \omega} + I_{a,j} Z_{self} + V^{ind}_{a,j} = 0 \tag{50}$$

$$-\frac{I^o_{a,j}}{i\, C_o\, \omega} + \frac{I^s_{a,j}}{i\, C_s\, \omega} + R_c\, (I_{a,j} + I^s_{a,j}) = 0 \tag{51}$$

$$\frac{I^o_{a,j}}{\imath\, C_o\, \omega} + I^L_{a,j} \left(\frac{1}{\imath\, C_T\, \omega} + Z_L + R_c\right) = 0 \tag{52}$$

$$I_{a,j}\, Z_{AB} + I_{a,j}\, Z_{self} + V^{ind}_{a,j} = 0 \tag{53}$$

where $Z_{AB} \equiv \widetilde{Z}_L$ defines the equivalent resistance between the nodes A and B and $I^L_{a,j} \equiv I_{a,j} + I^o_{a,j} + I^s_{a,j}$. $Z_{AB} \equiv \widetilde{Z}_L$ is found as follows by using (50-53):

$$\widetilde{Z}_L = \frac{-\lambda_4 - \lambda_5\, Z_L - \imath}{\omega\, (C_o + C_T + C_s + \imath\, \lambda_2 - \lambda_3 + \lambda_1\, Z_L)} \tag{54}$$

where and $\lambda_1 \equiv C_T\, \omega\, (-C_o\, C_s\, R_c\, \omega + \imath (C_o + C_s))$, $\lambda_2 \equiv R_c\, \omega\, (C_o (C_T + C_s) + 2\, C_T\, C_s)$, $\lambda_3 \equiv C_o\, C_T\, C_s\, R_c^2\, \omega^2$, $\lambda_4 \equiv -2\, C_T\, R_c\, \omega + C_o\, R_c\, \omega (-1 - \imath\, C_T\, R_c\, \omega)$ and $\lambda_5 \equiv C_T\, \omega\, (-1 - \imath\, C_o\, R_c\, \omega)$. The currents $I_{a,j}$, $I^o_{a,j}$ and $I^s_{a,j}$ are calculated as follows:

$$I_{a,j} = \frac{-\imath\, V^{ind}_{a,j}\, \omega\, (\imath\, \lambda_2 - \lambda_3 + \lambda_{12} + \lambda_1\, Z_L)}{\lambda_{10} + \lambda_{11}\, Z_L} \tag{55}$$

$$I^o_{a,j} = I_{a,j}\, \lambda_9 - \imath\, C_o\, V^{ind}_{a,j}\, \omega\, (-1 - \imath\, C_s\, R_c\, \omega) \tag{56}$$

$$I^s_{a,j} = -C_s\, \omega\, (I_{a,j}\, L\, \omega - \imath\, V^{ind}_{a,j}) + \imath\, C_s\, I_{a,j}\, R\, \omega \tag{57}$$

where $\lambda_6 \equiv C_o (R_c + R) + C_s\, R$, $\lambda_7 \equiv L\, (C_o + C_s) + C_o\, C_s\, R_c\, R$, $\lambda_8 \equiv C_o\, C_s\, L\, R_c$, $\lambda_9 \equiv C_o\, \omega\, (-\omega\, (C_s\, R_c\, R + L) + \imath\, (R_c + R)) - \imath\, \lambda_8\, \omega^3$, $\lambda_{10} \equiv 1 + \omega\, \left(\imath\, \xi_3 + \xi_5 - 2\, \imath\, \xi_4\, \omega^2 - \xi_2\, \omega\right)$, $\lambda_{11} \equiv C_T\, \omega\, \left(\lambda_8\, \omega^3 - \imath\, \lambda_7\, \omega^2 - \lambda_6\, \omega + \imath\right)$ and $\lambda_{12} \equiv C_o + C_T + C_s$.

The equalities for soma and synaptic coils are obtained with the same formulations for dendrite and axon coils, respectively while replacing $V_{d,j}$ and $V^{ind}_{d,j}$ with $V_{c,j}$ and $V^{ind}_{c,j}$, respectively, for the soma coils and replacing Z_L and $V^{ind}_{a,j}$ with Z_s and $V^{ind}_{s,j}$, respectively, for the synaptic coils.

REFERENCES

[1] A. Basu *et al.*, "Low-power, adaptive neuromorphic systems: Recent progress and future directions," *IEEE J. Emerg. Sel. Topics Circuits Syst.*, vol. 8, no. 1, pp. 6–27, Mar. 2018.

[2] B. Rajendran and F. Alibart, "Neuromorphic computing based on emerging memory technologies," *IEEE J. Emerg. Sel. Topics Circuits Syst.*, vol. 6, no. 2, pp. 198–211, Jun. 2016.

[3] A. B. Bilgin and O. B. Akan, "A fast algorithm for analysis of molecular communication in artificial synapse," *IEEE Trans. Nanobiosci.*, vol. 16, no. 6, pp. 408–417, Sep. 2017.

[4] S. S. Haykin, *Neural Networks and Learning Machines*, 3rd ed. Upper Saddle River, NJ, USA: Pearson, 2009.

[5] H. Li, T. F. Wu, S. Mitra, and H.-S. P. Wong, "Resistive RAM-centric computing: Design and modeling methodology," *IEEE Trans. Circuits Syst. I, Reg. Papers*, vol. 64, no. 9, pp. 2263–2273, Sep. 2017.

[6] D. Zhang *et al.*, "All spin artificial neural networks based on compound spintronic synapse and neuron," *IEEE Trans. Biomed. Circuits Syst.*, vol. 10, no. 4, pp. 828–836, Apr. 2016.

[7] D. Kuzum, R. G. D. Jeyasingh, B. Lee, and H.-S. P. Wong, "Nanoelectronic programmable synapses based on phase change materials for brain-inspired computing," *Nano Lett.*, vol. 12, no. 5, pp. 2179–2186, 2012.

[8] J. Grollier, D. Querlioz, and M. D. Stiles, "Spintronic nanodevices for bioinspired computing," *Proc. IEEE*, vol. 104, no. 10, pp. 2024–2039, Oct. 2016.

[9] M. M. Shulaker *et al.*, "Three-dimensional integration of nanotechnologies for computing and data storage on a single chip," *Nature*, vol. 547, pp. 74–78, Jul. 2017.

[10] M. A. Zidan, J. P. L. Strachan, and W. D. Lu, "The future of electronics based on memristive systems," *Nature Electron.*, vol. 1, no. 1, pp. 22–29, 2018.

[11] A. Avena-Koenigsberger, B. Misic, and O. Sporns, "Communication dynamics in complex brain networks," *Nature Rev. Neurosci.*, vol. 19, no. 1, pp. 17–33, 2018.

[12] D. Ielmini and H. S. P. Wong, "In-memory computing with resistive switching devices," *Nature Electron.*, vol. 1, no. 6, pp. 333–343, 2018.

[13] B. Gulbahar and G. Memisoglu, "MIComp: 3D on-chip magneto-inductive computing with simultaneous wireless information and power transfer," in *Proc. ACM Comput. Frontiers*, Ischia, Italy, May 2018, pp. 62–68.

[14] B. Gulbahar, "Theoretical analysis of magneto-inductive THz wireless communications and power transfer with multi-layer graphene nanocoils," *IEEE Trans. Mol. Biol. Multi-Scale Commun.*, vol. 3, no. 1, pp. 60–70, Mar. 2017.

[15] B. Gulbahar, "A communication theoretical analysis of multiple-access channel capacity in magneto-inductive wireless networks," *IEEE Trans. Commun.*, vol. 65, no. 6, pp. 2594–2607, Jun. 2017.

[16] B. Gulbahar, "Network topology modulation for energy and data transmission in Internet of magneto-inductive things," in *Proc. IEEE GLOBECOM 1st Int. Workshop Internet Everything (IoE)*, Washington, DC, USA, Dec. 2016, pp. 1–6.

[17] J. Kang *et al.*, "On-chip intercalated-graphene inductors for next-generation radio frequency electronics," *Nature Electron.*, vol. 1, pp. 46–51, Jan. 2018.

[18] D. A. Miller, "Attojoule optoelectronics for low-energy information processing and communications," *J. Lightw. Technol.*, vol. 35, no. 3, pp. 346–396, Feb. 2017.

[19] J. J. Harris, R. Jolivet, and D. Attwell, "Synaptic energy use and supply," *Neuron*, vol. 75, no. 5, pp. 762–777, 2012.

[20] B. Chanda, R. Blunck, L. C. Faria, F. E. Schweizer, I. Mody, and F. Bezanilla, "A hybrid approach to measuring electrical activity in genetically specified neurons," *Nature Neurosci.*, vol. 8, no. 11, pp. 1619–1626, 2015.

[21] L. R. Varshney, "Transporting information and energy simultaneously," in *Proc. IEEE Int. Symp. Inf. Theory*, Jul. 2008, pp. 1612–1616.

[22] A. Kansal, J. Hsu, S. Zahedi, and M. B. Srivastava, "Power management in energy harvesting sensor networks," *ACM Trans. Embedded Comput. Syst.*, vol. 6, no. 4, p. 32, Sep. 2007.

[23] Y. Urzhumov and D. R. Smith, "Metamaterial-enhanced coupling between magnetic dipoles for efficient wireless power transfer," *Phys. Rev. B, Condens. Matter*, vol. 83, no. 20, p. 205114, May 2011.

[24] B. Gulbahar, "Energy harvesting and magneto-inductive communications with molecular magnets on vibrating graphene and biomedical applications in the kilohertz to terahertz band," *IEEE Trans. Mol. Biol. Multi-Scale Commun.*, vol. 3, no. 3, pp. 194–206, Sep. 2017.

[25] P. W. Fowler, "How unusual is C_{60}? Magic numbers for carbon clusters," *Chem. Phys. Lett.*, vol. 131, no. 6, pp. 444–450, 1986.

[26] B. Gulbahar and O. B. Akan, "A communication theoretical modeling and analysis of underwater magneto-inductive wireless channels," *IEEE Trans. Wireless Commun.*, vol. 11, no. 9, pp. 3326–3334, Sep. 2012.

[27] Z. Wang *et al.*, "Q-factors of CVD monolayer graphene and graphite inductors," *J. Phys. D, Appl. Phys.*, vol. 50, no. 34, p. 345103, 2017.

[28] M. F. El-Kady and R. B. Kaner, "Scalable fabrication of high-power graphene micro-supercapacitors for flexible and on-chip energy storage," *Nature Commun.*, vol. 4, pp. 1–9, Feb. 2013.

[29] F. Xiong, A. D. Liao, D. Estrada, and E. Pop, "Low-power switching of phase-change materials with carbon nanotube electrodes," *Science*, vol. 332, no. 6029, pp. 568–570, 2011.

[30] J. Lee, M. Kim, and K. Yang, "A 1.52 THz RTD triple-push oscillator with μW-level output power," *IEEE Trans. THz Sci. Technol.*, vol. 6, no. 2, pp. 336–340, Mar. 2016.

[31] G. Carpintero, E. Garcia-Munoz, H. Hartnagel, S. Preu, and A. Raisanen, *Semiconductor Terahertz Technology: Devices and Systems at Room Temperature Operation*. Hoboken, NJ, USA: Wiley, 2015.

[32] P. A. Merolla *et al.*, "A million spiking-neuron integrated circuit with a scalable communication network and interface," *Science*, vol. 345, no. 6197, pp. 668–673, Aug. 2014.

[33] J. Han, C. Song, S. Gao, Y. Wang, C. Chen, and F. Pan, "Realization of the meminductor," *ACS Nano*, vol. 8, no. 10, pp. 10043–10047, 2014.

[34] J. H. Conway and N. J. A. Sloane, *Sphere Packings, Lattices and Groups*. New York, NY, USA: Springer-Verlag, 1998.

[35] H. Guo and Z. Sun, "M^2I communication: From theoretical modeling to practical design," in *Proc. IEEE Int. Conf. Commun.*, May 2016, pp. 1–6.

[36] S. Ambrogio *et al.*, "Unsupervised learning by spike timing dependent plasticity in phase change memory (PCM) synapses," *Frontiers Neuro-Sci.*, vol. 10, pp. 56-1–56-10, Mar. 2016.

[37] M. Prezioso, F. Merrikh-Bayat, B. D. Hoskins, G. C. Adam, K. K. Likharev, and D. B. Strukov, "Training and operation of an integrated neuromorphic network based on metal-oxide memristors," *Nature*, vol. 521, pp. 61–64, May 2015.



BURHAN GULBAHAR (M'12–SM'14) received the B.S. and M.S. degrees in electrical and electronics engineering from Bilkent University, Ankara, Turkey, in 1999 and 2002, respectively, and the Ph.D. degree in electrical and electronics engineering from Koc University, Istanbul, Turkey, in 2012. He was a Research Assistant with the Next-Generation and Wireless Communications Laboratory, Koc University. He is currently a Faculty Member with the Department of Electrical and Electronics Engineering, Ozyegin University, Istanbul, and the Director of the Applied Research Center of Technology Products, Ozyegin University. His current research interests include quantum computing and communications, neuromorphic computing, nanoscale design with 2D materials, nanoscale communications, the Internet-of-Things, and consumer electronics. He is a member of the ACM and a Senior Member of the IEEE Communications Society. He received the Finalist Award from the Bell Labs Prize 2015 Global Competition and the Faculty Information Transfer Excellence Award from Ozyegin University, in 2017, for the achievements in information transfer in national and international platforms.